Supporting Information

Selective Binding of Rare-Earth Ions in Polymerizable Cages

Jou-Tsen Ou[a] and Mercedes K. Taylor*[a]

[a]Department of Chemistry and Biochemistry, University of Maryland, College Park, MD 20742, United States

*E-mail: mkt@umd.edu

Table of Contents

General Methods

Materials: Anhydrous *N,N*-dimethylformamide (DMF) was obtained from an Inert solvent purification system. All other chemicals and solvents were purchased from chemical suppliers and were used without further purification.

Nuclear magnetic resonance (NMR) spectroscopy: Solution-state NMR spectra were collected on a Bruker 400 MHz and/or 600 MHz instruments. Chemical shifts are reported in parts per million (ppm) and are referenced to the solvent signal. Solid-state ^{13}C cross-polarization magic-angle spinning (CPMAS) NMR spectra were collected on a Bruker Avance NEO solid-state 500 MHz NMR spectrometer with a double resonance HX probe. Briefly, samples were packed in a 3.2 mm outer diameter zirconia rotor with Kel-F endcap spinning at 8-17 kHz (spectra in Fig. 3a in the manuscript were collected at 15 kHz). Proton-carbon matched cross polarization ramp was at 50 kHz with 2 ms contact time. The proton dipolar decoupling was achieved by applying continuous wave spinal64 on the ^{1}H channel during acquisition. The $\pi/2$ pulse length was 2.5 μs for ^{1}H and the recycle delay was 5 s. Carbon-13 chemical shifts were referenced with respect to TMS by setting $\delta(^{13}C) = 0$ ppm. The line broadening for the spectrum was 50 Hz.

Infrared spectroscopy (IR): Fourier transform infrared (FTIR) spectra were collected on Thermo Nicolet Nexus 670 FT-IR E.S.P. with an ATR probe. Data were obtained with solid samples using air from the room as a blank.

Mass spectrometry (MS): ESI spectra of cages were collected on a Bruker Maxis-II Q-TOF mass spectrometer equipped with an ESI ion source coupled with a Waters Acquity I-Class Plus LC system. The Maxis-II settings were as follows: endplate offset voltage = 500 V, capillary voltage = 4500 V, dry temperature = 220 °C, dry gas flow rate = 5.0 L/min, nebulizer gas pressure = 1.0 bar. The mass range in the measurement was from 400 to 3000 Da. For the elution, a mobile phase composed 0.1% formic acid in acetonitrile was used in the positive mode with the flow rate set to 0.15 mL/min. Simulations were performed with the Bruker Isotope Pattern software.

Small-angle X-Ray scattering (SAXS): SAXS measurements were collected on a Xenocs Xeuss system equipped with Cu Kα (wavelength ~ 1.54 Å). Each sample was placed in a capillary. Experiments were carried out for 15 minutes per sample at room temperature.

Scanning electron microscopy (SEM): SEM was performed on a Hitachi SU-70 FEG SEM instrument. Dry powders were deposited onto carbon tape and coated with gold and palladium.

Microwave plasma atomic emission spectrometer (MP-AES): Metal concentrations were measured using an Agilent Technologies 4210 MP-AES. The characteristic wavelengths, 398.852 nm and 488.368 nm, were used for lanthanum (La) and yttrium (Y), respectively. Data were analyzed using Agilent MP Expert software (version 1.6.1). Calibration curves for concentration determination were constructed using two standard solutions of elements in 1M nitric acid, along with a commercial calibration blank. All curves were fitted with rational function with error below 8% and correlation coefficient of 0.9999 or greater. Calibration standards were diluted gravimetrically from a commercial 1000 mg/L standard.

Synthetic Procedures

Synthetic route to L
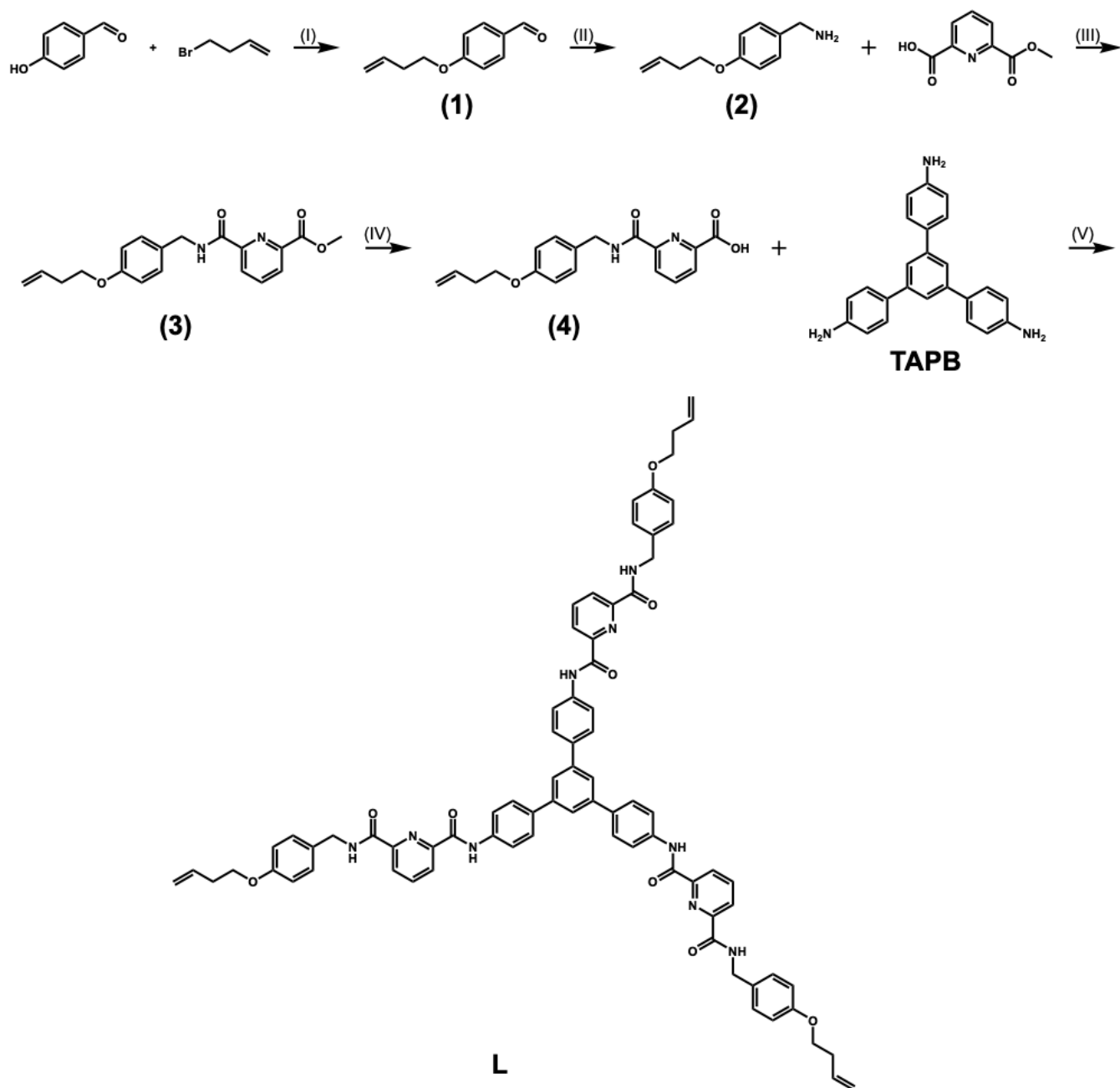
Scheme S1. Synthetic route to the ligand **L**. *Reagents and conditions:* (I) 4-hydroxybenzaldehyde, 4-bromobut-1-ene, potassium carbonate, sodium iodide, ethanol, 90 °C, 4 days, atmosphere of air. Yield = 57.7%. (II) hydroxylamine hydrochloride, pyridine, ethanol, 100 °C, 2 hours, atmosphere of air; zinc

powder, 2 N hydrochloric acid$_{(aq)}$, tetrahydrofuran, 80 °C, 3 hours, atmosphere of air. Yield = 87.1%. (III) 6-(methoxycarbonyl)picolinic acid, ethyl chloroformate, triethylamine, anhydrous dichloromethane (DCM), 30 °C, overnight, inert atmosphere. Yield = 74.8%. (IV) sodium hydroxide, water, methanol, DCM, 45 °C, overnight, atmosphere of air. Yield = 63.3%. (V) triethylamine, ethyl chloroformate, 1,3,5-tris-(4-aminophenyl)benzene (TAPB), anhydrous DCM, anhydrous N,N-dimethylformamide (DMF), 30 °C, overnight, inert atmosphere. Yield = 55.4%.
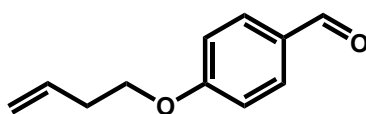
Fig. S1. The molecular structure of **(1)**

Synthesis of (1): Adapted from literature procedures,[1] 4-hydroxybenzaldehyde (12.2 g, 100 mmol, 1.0 equiv), 4-bromobut-1-ene (12.2 mL, 120 mmol, 1.2 equiv), potassium carbonate (20.7 g, 150 mmol, 1.5 equiv), sodium iodide (18.0 g, 120 mmol, 1.2 equiv), and ethanol (532 mL) were combined in a single-neck round-bottom flask at room temperature. The reaction mixture was then refluxed at 90 °C for 4 days. Upon completion, the mixture was filtered and washed with approximately 200 mL of ethanol. The filtrate was concentrated by rotary evaporation, and the residue was extracted with ethyl acetate and deionized (DI) water. The organic solution was dried over magnesium sulfate, filtered, and concentrated by rotary evaporation, yielding the product **(1)** as a yellow oil. Yield: 10.2 g, 57.7%. ^{1}H NMR (400 MHz, CDCl$_3$, 298 K): δ = 9.88 (s, 1H), 7.84–7.82 (d, J = 8.8 Hz, 2H), 7.01–6.99 (d, J = 8.7 Hz, 2H), 5.95–5.85 (m, 1H), 5.21–5.17 (d, J = 17.2 Hz, 1H), 5.15–5.12 (d, J = 10.2 Hz, 1H), 4.12–4.08 (t, J = 6.7 Hz, 2H), 2.61–2.56 (m, 2H) ppm.
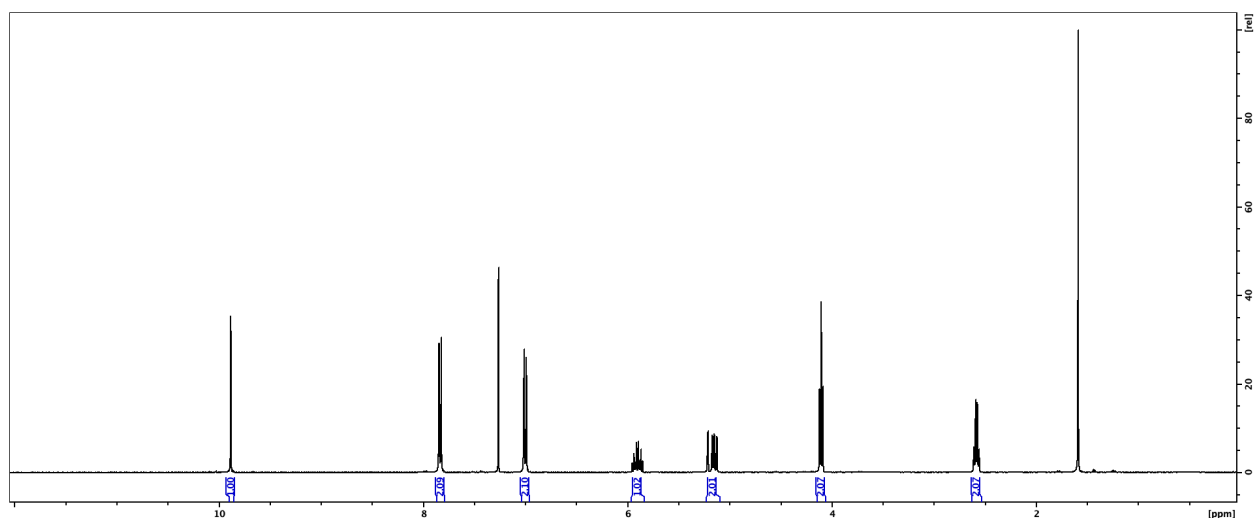
Fig. S2. ^{1}H NMR spectrum of **(1)** (400 MHz, CDCl₃, 298 K).
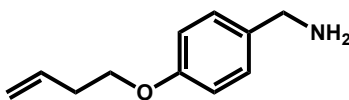
Fig. S3. The molecular structure of **(2)**.

Synthesis of (2): Adapted from literature procedures,[1] **(1)** (10.2 g, 57.7 mmol, 1.0 equiv), hydroxylamine hydrochloride (6.0 g, 86.6 mmol, 1.5 equiv), pyridine (5.6 mL, 69.3 mmol, 1.2 equiv), and ethanol (122 mL) were combined in a single-neck round-bottom flask. The reaction mixture was then refluxed at 100 °C for 2 hours. Upon completion, the mixture was concentrated by rotary evaporation, and the residue was extracted with ethyl acetate and DI water. The organic solution was dried over magnesium sulfate, filtered, and concentrated by rotary evaporation. The mixture was further purified with column chromatography (ethyl acetate = 10%, in hexanes), affording the intermediate oxime E/Z isomers. The intermediate oxime, zinc powder (37.2 g, 569 mmol, 9.9 equiv), 2 N hydrochloric acid₍ₐq₎ (149 mL), and tetrahydrofuran (369 mL) were then combined in a single-neck round-bottom flask, and the reaction mixture was heated at 80 °C for 3 hours attached with a reflux condenser. Upon completion, the mixture

S6

was cooled down to the room temperature and filtered through celite to remove zinc. The filtrate was concentrated by rotary evaporation to remove tetrahydrofuran, and 28-30% ammonium hydroxide was added to raise the pH value above 8, which led to the precipitation of white solids. The precipitate was filtered and washed with approximately 150 mL of DI water, ~50 mL of ethyl ether, and ~100 mL of ethyl acetate. The product was obtained as a white solid (**2**). The decomposition range was measured to be 282-290 °C. No melting transition was observed before the decomposition transition. Yield: 8.90 g, 87.1%. ^{1}H NMR (400 MHz, DMSO-d_6, 298 K): δ = 7.27–7.24 (d, J = 8.6 Hz, 2H), 6.88–6.86 (d, J = 8.6 Hz, 2H), 5.93–5.83 (m, 1H), 5.18–5.13 (d, J = 17.3 Hz, 1H), 5.09–5.06 (d, J = 10.4 Hz, 1H), 4.00–3.97 (t, J = 6.6 Hz, 2H), 3.64 (s, 2H), 3.37 (s, 2H), 2.48–2.43 (m, 2H) ppm.
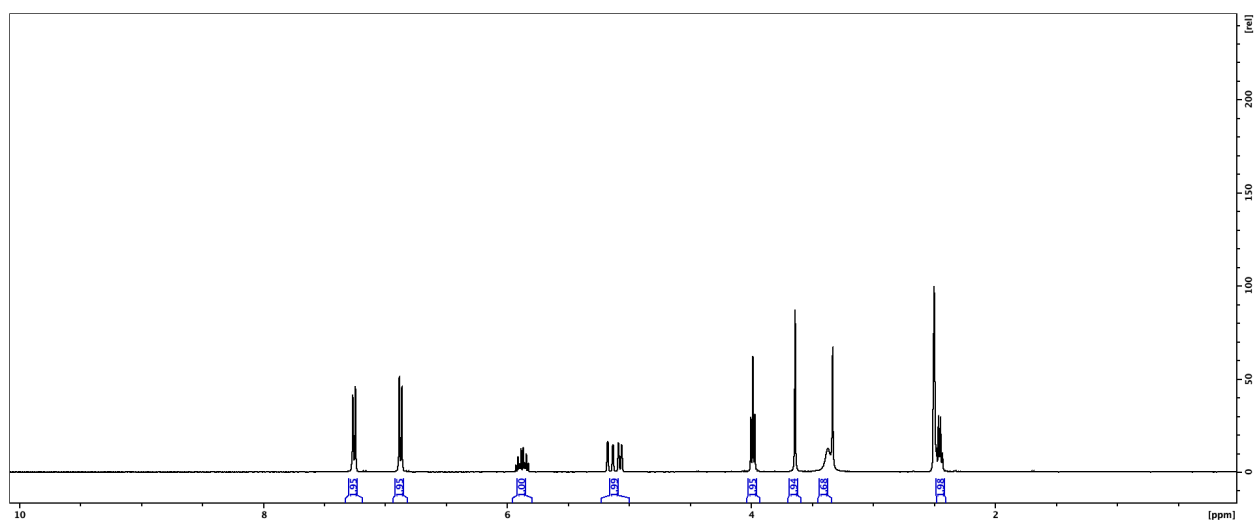
Fig. S4. ^{1}H NMR spectrum of (**2**) (400 MHz, DMSO-d_6, 298 K).
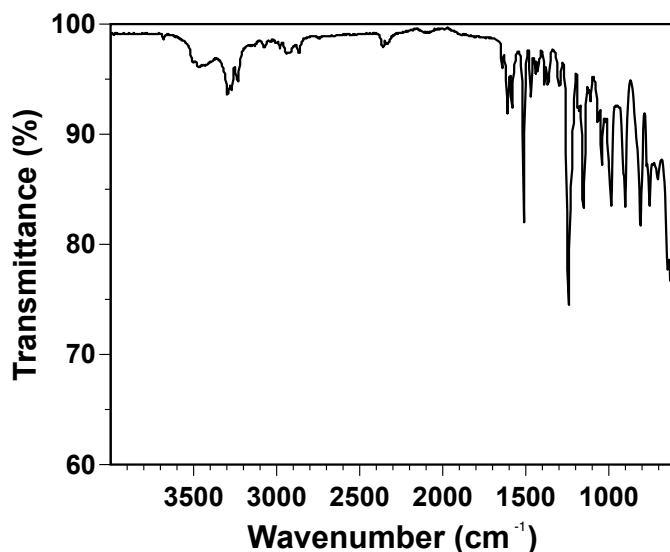
Fig. S5. Infrared (IR) spectrum of **(2)**.
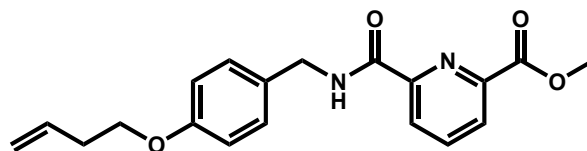
Fig. S6. The molecular structure of **(3)**.

Synthesis of (3): Adapted from literature procedures,[2] 6-(methoxycarbonyl)picolinic acid (8.21 g, 45.3 mmol, 1.1 equiv) was dissolved in anhydrous dichloromethane (DCM; 271 mL) in an oven-dried round-bottom flask at room temperature under an inert atmosphere, followed by the addition of triethylamine (6.9 mL, 49.4 mmol, 1.2 equiv). Ethyl chloroformate (5.9 mL, 61.8 mmol, 1.5 equiv) was added, and the mixture was then stirred at room temperature for 30 min to form the anhydride intermediate. Compound **(2)** (7.30 g, 41.2 mmol, 1.0 equiv) and triethylamine (11.5 mL, 82.4 mmol, 2.0 equiv) were added into the anhydride solution at 30 °C under inert atmosphere. The reaction mixture was then stirred for 30 min, and triethylamine (6.9 mL, 49.4 mmol, 1.2 equiv) and ethyl chloroformate (5.9 mL, 61.8 mmol, 1.5 equiv) were added into the solution again at 30 °C under inert atmosphere. The reaction mixture was then stirred

overnight at 30 °C. Upon completion, the reaction was exposed to air and concentrated by rotary evaporation. The residue was extracted with ethyl acetate and water, and the organic layer was dried over magnesium sulfate, filtered, and concentrated by rotary evaporation. The mixture was further purified with column chromatography (ethyl acetate = 30%–50% gradient, in hexanes), yielding the product (3) as a colorless oil. Yield: 10.5 g, 74.8%. ^{1}H NMR (400 MHz, CDCl$_3$, 298 K): δ = 8.43–8.41 (d, J = 7.8 Hz, 1H), 8.39–8.36 (t, J = 6.0 Hz, 1H), 8.23–8.21 (d, J = 7.8 Hz, 1H), 8.03–7.99 (t, J = 7.8 Hz, 1H), 7.30–7.28 (d, J = 8.7 Hz, 2H), 6.88–6.86 (d, J = 8.7 Hz, 2H), 5.94–5.84 (m, 1H), 5.18–5.14 (d, J = 17.2 Hz, 1H), 5.11–5.09 (d, J = 10.3 Hz, 1H), 4.63–4.62 (d, J = 6.2 Hz, 2H), 4.02–3.98 (t, J = 6.7 Hz, 2H), 3.98 (s, 3H), 2.56–2.51 (m, 2H) ppm.
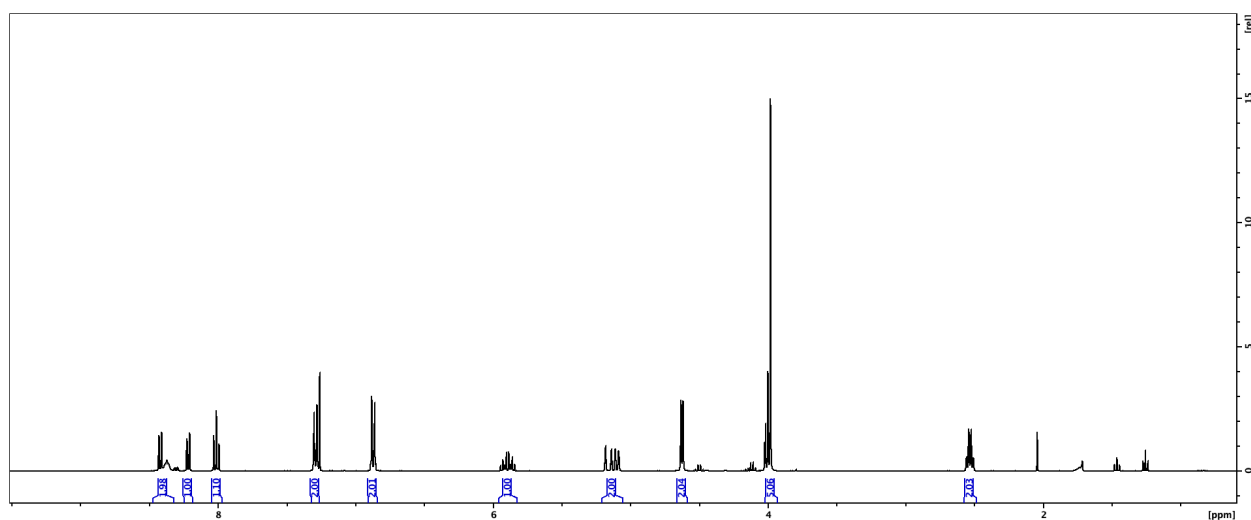
Fig. S7. ^{1}H NMR spectrum of (3) (400 MHz, CDCl$_3$, 298 K).
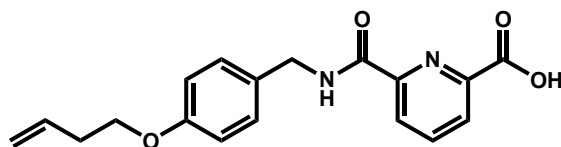
Fig. S8. The molecular structure of (4).

Synthesis of (4): Adapted from literature procedures,[3] compound **(3)** (5.85 g, 17.2 mmol, 1.0 equiv) was dissolved in a mixture of methanol (240 mL) and DCM (362 mL) in a single-neck round-bottom flask. Sodium hydroxide (2.8 g, 68.8 mmol, 4.0 equiv) and DI water (2.5 mL, 138 mmol, 8.0 equiv) were added to the solution at room temperature. The mixture was refluxed at 45 °C overnight. The solution was then cooled to room temperature and concentrated by rotary evaporation. The residue was dissolved in DI water, and the solution was filtered with DI water. The filtrate was acidified by adding 1 N HCl aqueous solution until the pH value reached ~1, which caused white solids to precipitate. The suspension was left in a fridge for 4 hr, and the suspended solids were isolated by filtration and washed with approximately 100 mL of DI water and then ~100 mL of ethyl acetate. The product was obtained as a white solid **(4)** after filtration. The melting point range was measured to be 110-112 °C. Yield: 3.55 g, 63.3%. ^{1}H NMR (400 MHz, DMSO-d_6, 298 K): δ = 13.07 (s, 1H), 9.67–9.64 (t, J = 6.2 Hz, 1H), 8.31–8.20 (m, 3H), 7.27–7.25 (d, J = 8.6 Hz, 2H), 6.91–6.89 (d, J = 8.7 Hz, 2H), 5.92–5.82 (m, 1H), 5.17–5.13 (d, J = 17.3 Hz, 1H), 5.08–5.05 (d, J = 10.3 Hz, 1H), 4.51–4.50 (d, J = 6.2 Hz, 2H), 4.01–3.97 (t, J = 6.6 Hz, 2H), 2.48–2.43 (m, 2H) ppm.
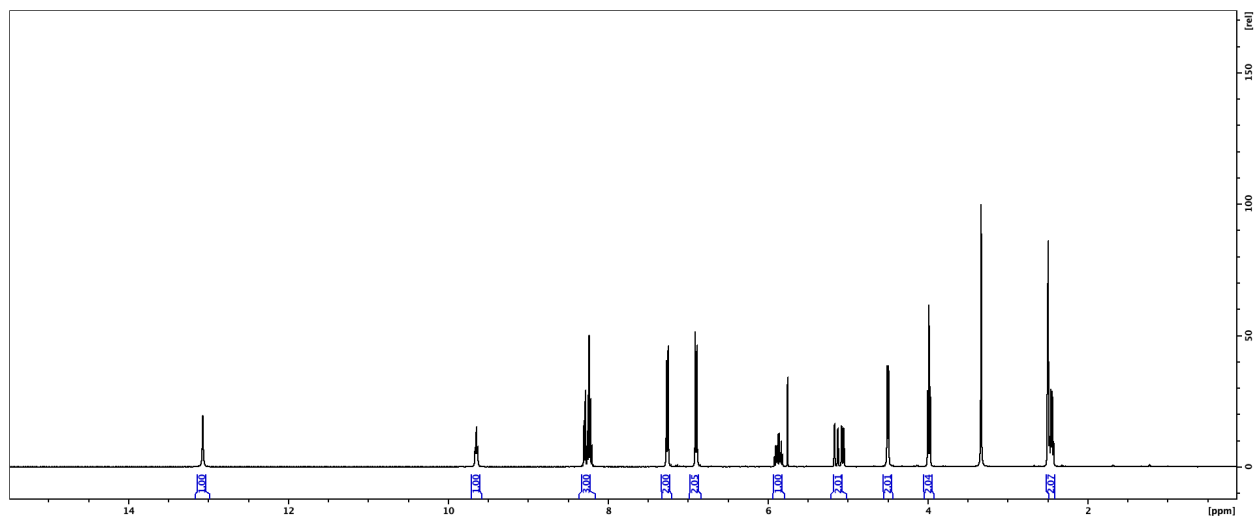
Fig. S9. ^{1}H NMR spectrum of **(4)** (400 MHz, DMSO-d_6, 298 K).
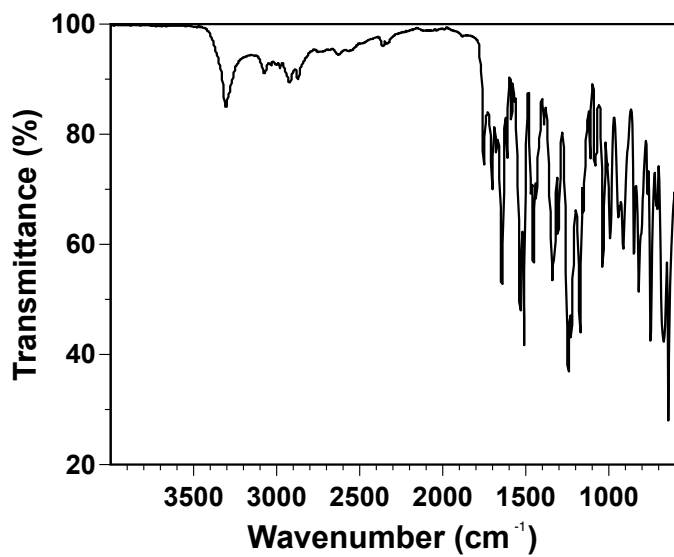
Fig. S10. Infrared (IR) spectrum of (**4**).
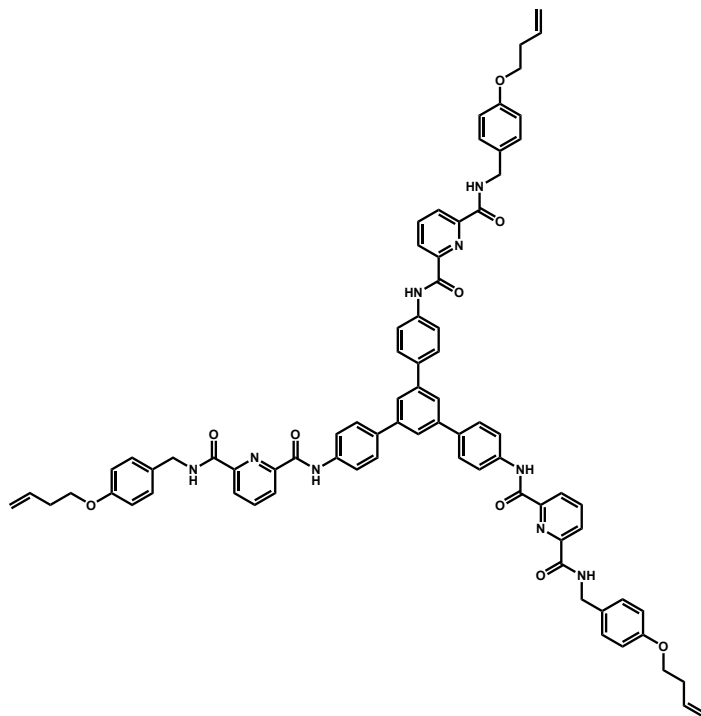
Fig. S11. The molecular structure of **L**.

Synthesis of L: Adapted from literature procedures,[2] compound **(4)** (1.34 g, 4.0 mmol, 4.0 equiv) was dissolved in anhydrous DCM (30 mL) in an oven-dried round-bottom flask at room temperature under an inert atmosphere, followed by the addition of triethylamine (1.0 mL, 7.0 mmol, 7.0 equiv). Ethyl chloroformate (0.65 mL, 7.0 mmol, 7.0 equiv) was added, and the mixture was stirred at room temperature for 30 min to form the anhydride intermediate. TAPB (0.35 g, 1.0 mmol, 1.0 equiv), triethylamine (0.55 mL, 4.0 mmol, 4.0 equiv), and DMF (5 mL) were added into the anhydride solution at 30 °C under inert atmosphere. The reaction mixture was then stirred for 30 min, and triethylamine (1.0 mL, 7.0 mmol, 7.0 equiv) and ethyl chloroformate (0.65 mL, 7.0 mmol, 7.0 equiv) were added into the solution again at 30 °C under inert atmosphere. The reaction mixture was stirred overnight at 30 °C. Upon completion, the reaction was exposed to air and concentrated by rotary evaporation. The residue was suspended in DI water, and the suspension was stirred for several hours. The suspended solids were isolated by filtration and washed with water and ethyl ether. The solids were dissolved in DCM, ethyl acetate and ethyl ether were added to precipitate out the product, and the suspension was stirred for several hours. The suspended solids were isolated by filtration and washed with approximately 50 mL of ethyl acetate and approximately 50 mL ethyl ether. The solids were again suspended in DCM, ethyl acetate and ethyl ether were added, and the suspension was stirred overnight. The suspended solids were isolated by filtration and washed with approximately 50 mL of ethyl acetate and approximately 50 mL ethyl ether. The white solid product (**L**) was obtained after filtration. The melting point range was measured to be 168-170 °C. Yield = 0.707 g, 55.4%. ^{1}H NMR (400 MHz, DMSO-d_6, 298 K): δ = 10.91 (s, 3H), 10.03–10.00 (t, J = 6.1 Hz, 3H), 8.40–8.25 (m, 9H), 8.00–7.96 (m, 15H), 7.32–7.30 (d, J = 8.4 Hz, 6H), 6.93–6.91 (d, J = 8.5 Hz, 6H), 5.92–5.82 (m, 3H), 5.17–5.12 (d, J = 17.4 Hz, 3H), 5.07–5.05 (d, J = 10.2 Hz, 3H), 4.60–4.59 (d, J = 5.6 Hz, 6H), 4.01–3.98 (t, J = 6.5 Hz, 6H), 2.48–2.43 (m, 6H) ppm. ^{13}C NMR (400 MHz, DMSO-d_6, 298 K):

δ = 163.27, 161.76, 157.53, 149.04, 148.64, 141.05, 139.83, 137.60, 136.09, 134.93, 131.36, 128.55, 127.43, 125.09, 124.94, 123.59, 121.79, 117.01, 114.41, 66.68, 41.83, 33.1 ppm.
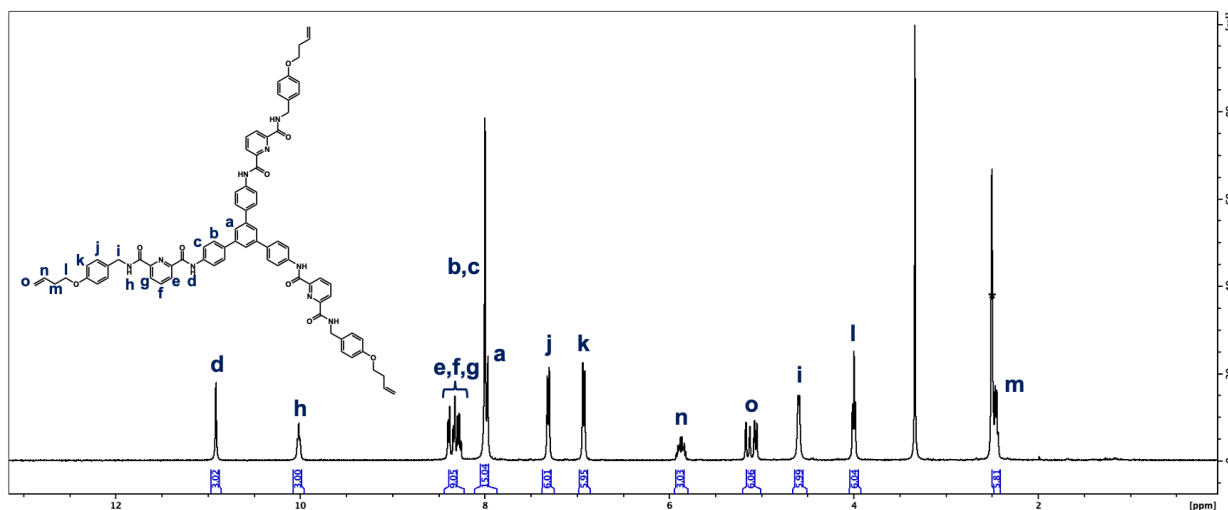
Fig. S12. ^{1}H NMR spectrum of **L** (400 MHz, DMSO-d_6, 298 K). Because the peaks at 10.91 ppm and 10.03-10.00 ppm (peaks **d** and **h**) are not coupled to any carbons in the HSQC NMR spectrum (Fig. S13), they are assigned to be amide hydrogens. Since peak **d** is a singlet while peak **h** is a triplet, peak **d** is assigned as the amide H close to the TAPB core and peak **h** is assigned as the amide H closer to the terminal alkene. Because the multiplet at 8.40–8.25 ppm has the integration with 9 hydrogens, and because these hydrogens are coupled to each other in the COSY NMR spectrum (Fig. S12.), they are assigned as the aromatic hydrogens on the pyridine ring. Because the multiplet at 8.00–7.96 ppm (**a-c**) has the integration with 15 hydrogens, and because these hydrogens are coupled to each other in the COSY NMR spectrum (Fig. S12.), they are assigned to be the aromatic hydrogens on the center of the TAPB ring. The two doublets at 7.32–7.30 ppm (**j**) and 6.93–6.91 ppm (**k**) are assigned to be on the aromatic ring closer to the terminal alkene. The multiplet (**n**) at 5.92–5.82 ppm and the two doublets (**o**) at 5.17–5.12 ppm and 5.07–5.05 ppm have the integration ratio 3:3:3; they are assigned as the alkene hydrogens. Since the doublet (**i**) at 4.60–4.59 ppm is coupled to amide hydrogen (**h**) in the COSY NMR spectrum, the doublet is assigned as the H atoms on the aliphatic carbon next to the amide. Since the triplet (**l**) at 4.01–3.98 ppm

is coupled to the multiplet (**m**) at 2.48–2.43 ppm, which is coupled to alkene hydrogen **n** in the COSY NMR spectrum, hydrogen (**l**) is assigned to be next to the ether and hydrogen (**m**) is assigned to be next to the hydrogen (**n**).
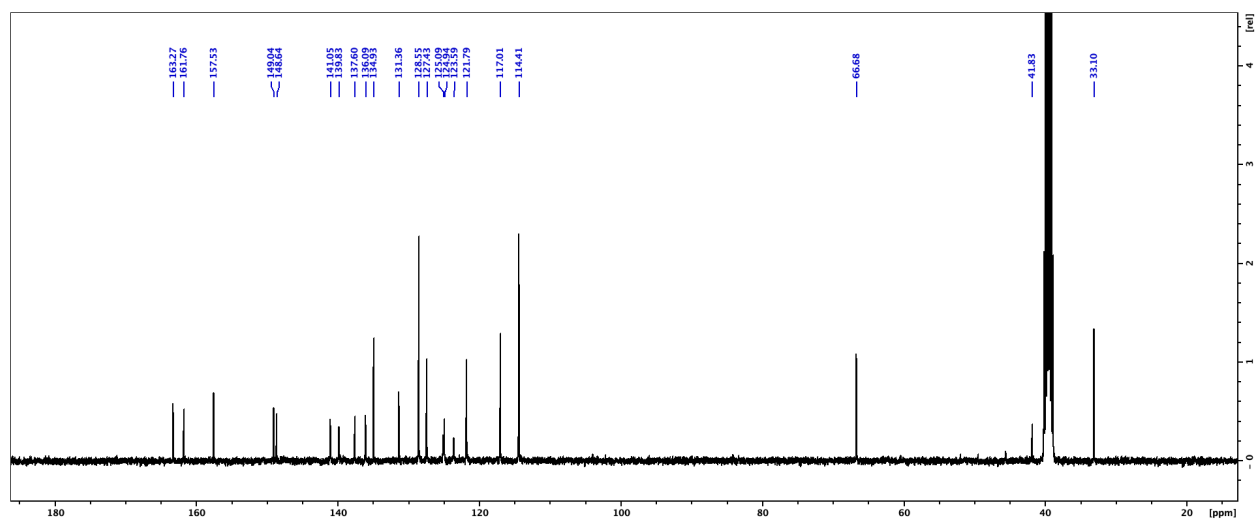
Fig. S13. ^{13}C NMR spectrum of **L** (400 MHz, DMSO-d_6, 298 K).
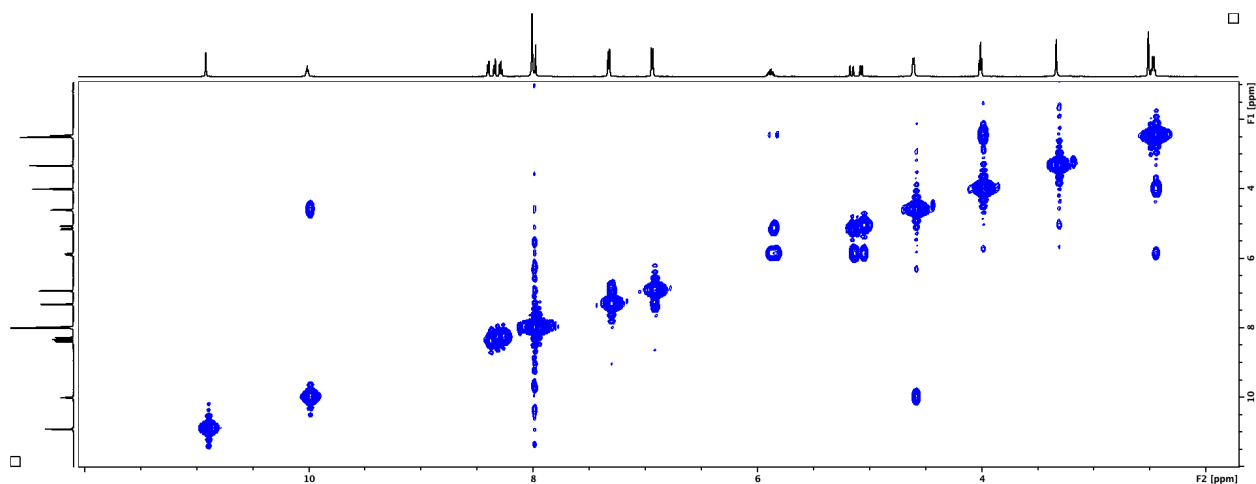
Fig. S14. COSY NMR spectrum of **L** (600 MHz, DMSO-d_6, 298 K).
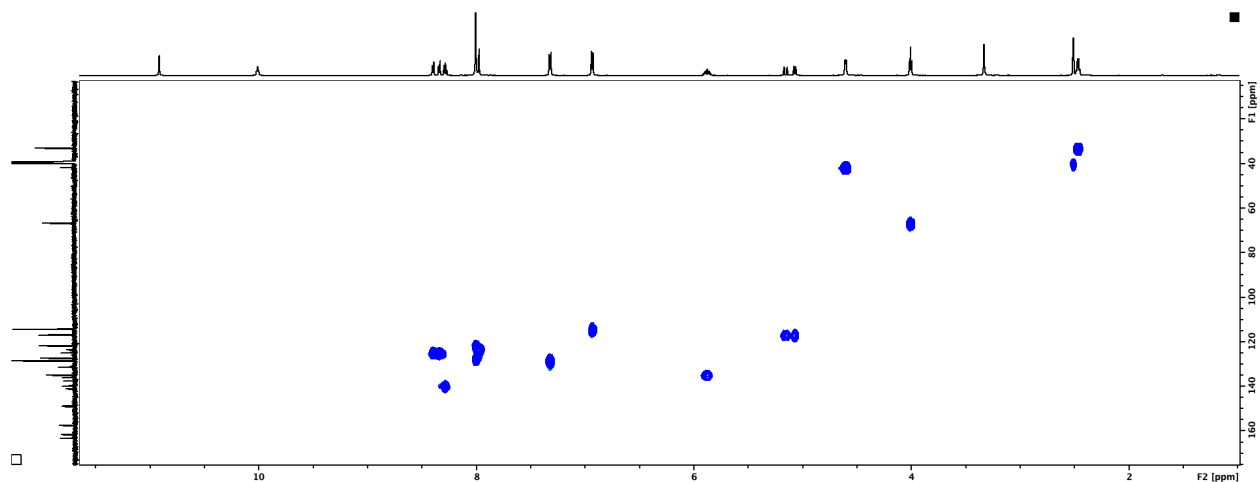
Fig. S15. HSQC NMR spectrum of **L** (600 MHz, DMSO-*d₆*, 298 K).
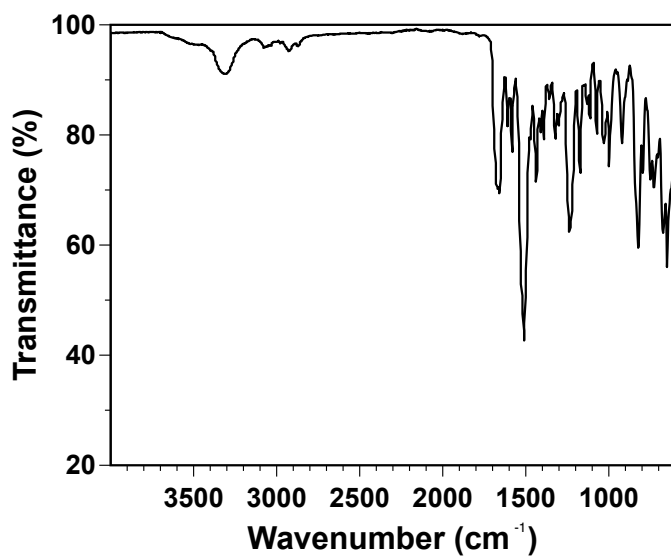
Fig. S16. Infrared (IR) spectrum of **L**.

Synthetic route to TAPB
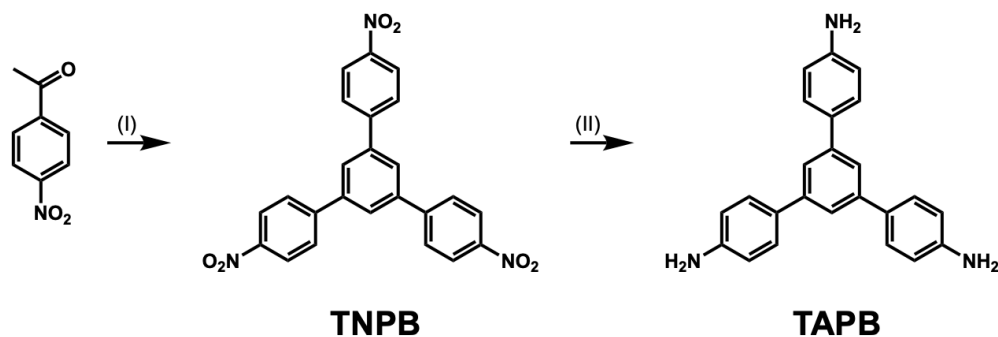
Scheme S2. Synthetic route to 1,3,5-tris-(4-aminophenyl)benzene (TAPB). *Reagents and conditions:* (I) *p*-nitroacetophenone, trifluoromethanesulfonic acid, toluene, 130 °C, three days, atmosphere of air. (II) absolute ethanol, 10% Pd on carbon, hydrazine monohydrate, 100 °C, two days, atmosphere of air. Yield = 80.9%.
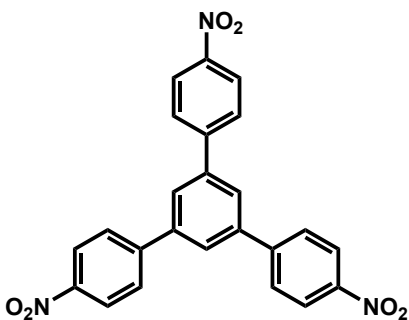
Figure S17. The molecular structure of 1,3,5-tris(4-nitrophenyl)benzene (TNPB).

Synthesis of 1,3,5-tris(4-nitrophenyl)benzene (TNPB): Adapted from literature procedures,[4,5] *p*-nitroacetophenone (50.0 g, 303 mmol, 1.0 equiv) was suspended in toluene (202 mL) in a single-neck round-bottom flask equipped with a Dean-Stark apparatus with a cooling condenser at room temperature, followed by the addition of trifluoromethanesulfonic acid (5.0 mL, 57 mmol, 0.19 equiv). The mixture was refluxed at 130 °C for three days. The reaction mixture was then cooled down to at room temperature

and filtered with a large amount of acetone. The residue was washed with DMF in a Soxhlet extractor for ~3 days until the solid turned yellow-green. The solids were washed with acetone, and the product TNPB was obtained after filtration as a yellow-green solid, in accordance with previous reports.[4,5] Yield: 18.6 g. The melting point range was measured to be higher than 400 °C. Because TNPB is not soluble in most common solvents, the NMR spectrum is not available.
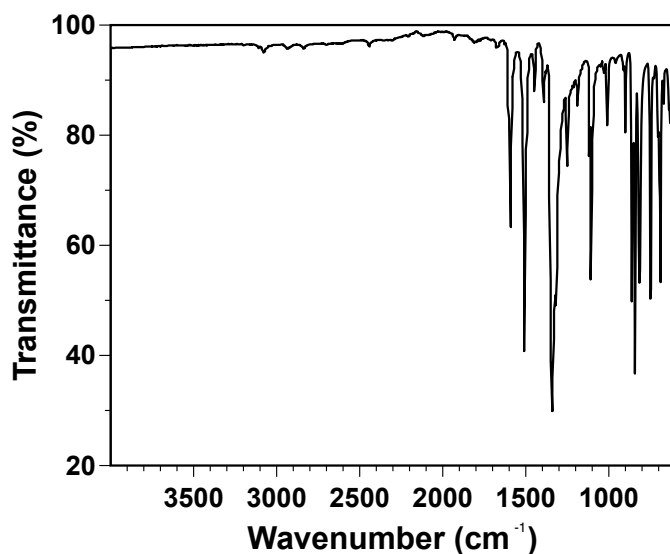
Fig. S18. Infrared (IR) spectrum of TNPB.
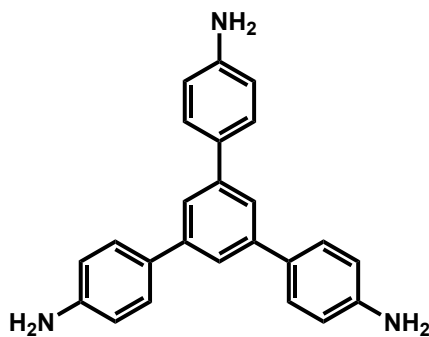
Figure S19. The molecular structure of TAPB.

Synthesis of 1,3,5-tris-(4-aminophenyl)benzene (TAPB): Safety note – Dry Pd on carbon (Pd/C) can ignite in the presence of air and organic solvent. Adapted from literature procedures,[4,5] TNPB (31.3 g, 71.0 mmol, 1.0 equiv) was suspended in absolute ethanol (850 mL), followed by the addition of 10% Pd on carbon (3.02 g) and hydrazine monohydrate (300 mL) at room temperature. The suspension was stirred 100 °C for two days. The reaction mixture was then filtered through celite while still hot, and the filtrate was concentrated by rotary evaporation, causing a red-orange precipitate to form. The precipitate was filtered and washed with approximately 500 mL of ethanol. The precipitate was then suspended in refluxing ethanol for approximately 3 hours and filtered to yield the product TAPB as a yellow solid. The melting point range was measured to be 259-262 °C. Yield: 20.2 g, 80.9%. ^{1}H NMR (600 MHz, DMSO-d_6, 298 K): δ = 7.48 (s, 3H), 7.48–7.46 (d, J = 8.5 Hz, 6H), 6.67–6.66 (d, J = 8.5 Hz, 6H), 5.21 (s, 6H) ppm.
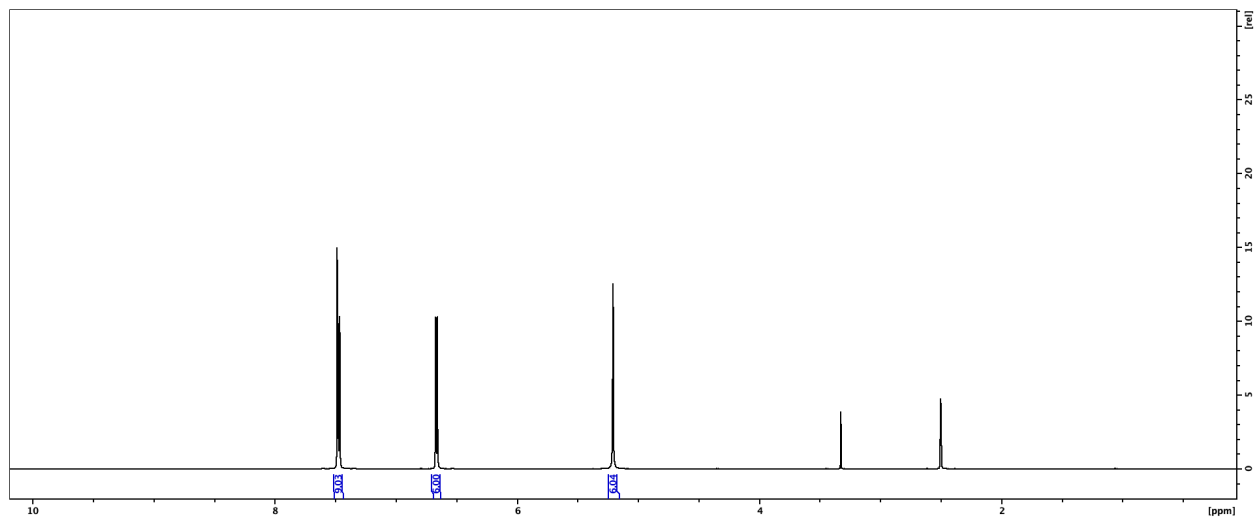
Figure S20. ^{1}H NMR spectrum of TAPB (600 MHz, DMSO-d_6, 298 K).
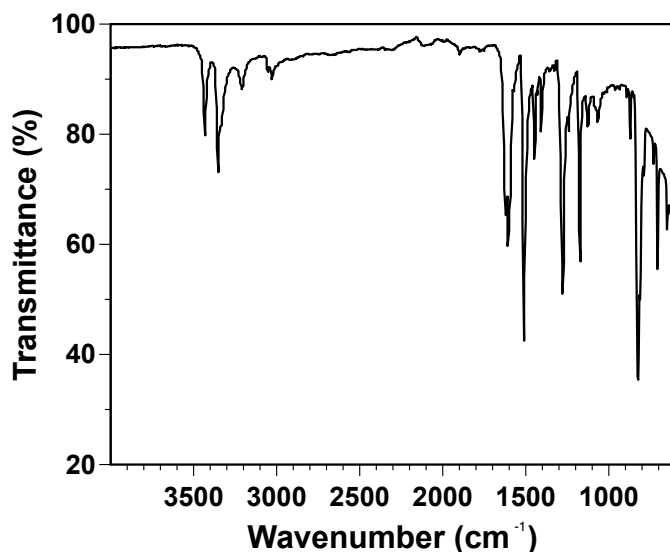
Fig. S21. Infrared (IR) spectrum of TAPB.

Synthetic route to M$_4$L$_4$ cages

Synthesis of Y$_4$L$_4$ cage: Adapted from literature procedures,[3] the ligand **L** (12.8 mg, 0.01 mmol, 1.0 equiv), yttrium(III) trifluoromethanesulfonate (Y(III) triflate, Y(OTf)$_3$; 5.9 mg, 0.011 mmol, 1.1 equiv), and acetonitrile (0.6 mL) were combined in 2.0 mL vial. (If subsequent NMR experiments were planned, deuterated acetonitrile (0.6 mL) was used as a solvent.) The reaction mixture was heated at 80 °C without stirring for three hours. The reaction mixture was then cooled to room temperature, yielding the Y$_4$L$_4$ cage solution. Results of C/H/N combustion analysis are as follows. Calculated: Carbon (C%) = 53.67%; hydrogen (H%) = 3.84%; nitrogen (N%) = 6.95%; found: C% = 53.14%; H% = 3.65%; N% = 6.93%. Results of inductively coupled plasma optical emission spectrometry (ICP-OES) analysis for yttrium content are as follows. Calculated: Yttrium (Y%) = 4.90%.; found: Y% = 4.64%. The theoretical chemical formula of Y$_4$L$_4$ cage is C$_{324}$H$_{276}$N$_{36}$O$_{72}$F$_{36}$S$_{12}$Y$_4$.

The synthesis of analogous M_4L_4 cages containing europium (Eu^{3+}), terbium (Tb^{3+}), dysprosium (Dy^{3+}), holmium (Ho^{3+}), or lanthanum (La^{3+}) metal ions were conducted under the same conditions as for yttrium (above), using triflate salts of the respective metal ions. For example, europium(III) triflate ($Eu(OTf)_3$) was used to synthesize Eu_4L_4 cage.
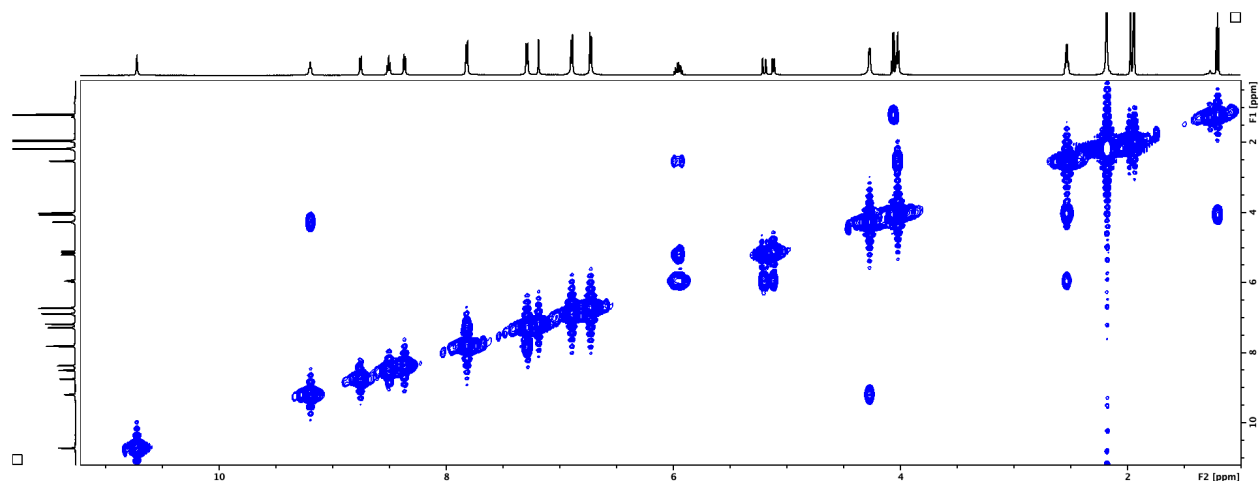
Fig. S22. COSY NMR spectrum of Y_4L_4 cage (600 MHz, CD_3CN, 298 K).

Synthetic route to the network of Y_4L_4 cages

Synthesis of network of Y_4L_4 cages (1:1 alkene:thiol): The Y_4L_4 cage was first synthesized at the following scale: **L** (38.3 mg, 0.03 mmol, 1.0 equiv), $Y(OTf)_3$ (17.7 mg, 0.033 mmol, 1.1 equiv), and acetonitrile (1.8 mL) were combined at 80 °C without stirring for three hours. Separately from the cage synthesis, 1,4-butanedithiol (5.5 mg, 0.045 mmol, 1.5 equiv) and 2,2'-azobis(2-methylpropionitrile) (AIBN) (5.7 mg, 5% weight percent per vinyl group) were combined in a single-neck round-bottom flask. The Y_4L_4 cage solution was then transferred to the round-bottom flask, the solvent of the mixture was removed by rotary evaporation, and acetonitrile (1.0 mL) was added to the flask. The flask was equipped with a condenser, and the mixture was stirred at 70 °C under inert atmosphere overnight. The reaction mixture was then cooled to room temperature. Acetonitrile was added into the round-bottom flask, and the reaction mixture

was stirred for 30 minutes. The mixture was filtered, and the solids were washed with ~10 mL of each of the following solvents: acetonitrile, chloroform, ethyl acetate, and methanol. The solids were washed until only solvent signals were observed in the NMR experiments with DMSO-d_6. The product was collected as a yellow solid. Yield: 33.7 mg.

Synthesis of network of Y$_4$L$_4$ cages (1:10 alkene:thiol): The synthetic procedure was the same as the synthesis of network of Y$_4$L$_4$ cages (1:1 alkene:thiol), except for the use of excess 1,4-butanedithiol (55 mg, 0.45 mmol, 15 equiv) in the synthesis. The product was collected as a yellow solid. Yield: 33.2 mg.

Procedure for mixed-metal binding experiments

The mixed-metal binding experiment for La^{3+}/Ho^{3+}: Adapted from literature procedures,[6] the procedure was the same as the synthesis of Y$_4$L$_4$ cage described above, except that a binary mixture of the metal salts La(OTf)$_3$ (5.9 mg, 0.01 mmol, 1.0 equiv) and Ho(OTf)$_3$ (6.1 mg, 0.01 mmol, 1.0 equiv) was used in place of Y(OTf)$_3$.

A series of other mixed-metal binding experiments was conducted under the same reaction conditions with different binary combinations of metal salts. Overall, fourteen experiments were conducted, using the following combinations: La^{3+}/Ho^{3+}, La^{3+}/Y^{3+}, La^{3+}/Dy^{3+}, La^{3+}/Tb^{3+}, La^{3+}/Eu^{3+}, Eu^{3+}/Ho^{3+}, Eu^{3+}/Y^{3+}, Eu^{3+}/Dy^{3+}, Eu^{3+}/Tb^{3+}, Tb^{3+}/Ho^{3+}, Tb^{3+}/Y^{3+}, Tb^{3+}/Dy^{3+}, Dy^{3+}/Y^{3+}, and Y^{3+}/Ho^{3+}.

Synthetic route to demetallated network scaffolds

Synthesis of demetallated network scaffold (1:1): The network of Y$_4$L$_4$ cages (1:1 alkene:thiol; 118 mg) was suspended in 1.0 mL cesium fluoride solution (CsF) in methanol (100 mg CsF in 1.0 mL methanol)

in a centrifugate tube. The suspension was sonicated for 30 min at room temperature. After centrifugation, the solids were collected by filtration and suspended in CsF solution again. The preparation of suspension and sonication were repeated three times. The solids were then filtered and washed with ~5 mL of methanol and ~5 mL of ethyl ether. The product was collected as a white solid. Yield: 88 mg.

Synthesis of demetallated network scaffold (1:10): The synthetic procedure was the same as the network scaffold (1:10), except for the use of the network of Y_4L_4 cages (1:10 alkene:thiol; 140.5 mg) in the synthesis. The product was collected as a white solid. Yield: 117.6 mg.

Procedure for the rare-earth adsorption experiments

Single-metal adsorption experiments for Y^{3+} or La^{3+}: The Y^{3+} or La^{3+} stock solutions were prepared by dissolving $Y(OTf)_3$ (107.4 mg) or $La(OTf)_3$ (120.8 mg) in 9.57 g and 9.50 g methanol, respectively. The network scaffolds (~14-15 mg) were suspended in ~0.6 mL of a given stock solution. The suspension was stirred and heated at 55 °C for three hours. The suspension was then centrifuged, and the supernatant was collected. The remaining solids were suspended in methanol, the suspension was centrifuged again, and the supernatant was collected and combined with the first fraction of supernatant. The methanol washing and centrifugation step was repeated twice. The combined fractions of supernatant were concentrated by rotary evaporation, and the residue was dissolved in 1.0 mL of 1.0 M nitric acid$_{(aq)}$ and 9.0 mL of DI water. The solution was filtered, and the concentration of the filtrate was determined by the MP-AES.

Mixed-ion adsorption experiments for Y³⁺/La³⁺: The procedure was the same as the procedure for single-ion experiments, except that a stock solution containing a binary mixture of Y^{3+}/La^{3+} was prepared by dissolving both Y(OTf)₃ (116.8 mg) and La(OTf)₃ (121.7 mg) in 9.63 g methanol.

These conditions were chosen to be as similar to the cage synthesis conditions as possible while ensuring the solubility of the rare-earth ions (which are insoluble in the cage synthesis solvent, acetonitrile). Therefore methanol was selected as the solvent for the ion adsorption experiments, and these experiments were carried out at 55 °C in order to remain below the boiling point of methanol.

Calculation of Dynamic Radius Based on Stokes-Einstein Equation

Stokes-Einstein equation used for the diffusion coefficient is $D = k_B T/6\pi\eta r$, where k_B is the Boltzmann constant ($1.38*10^{-23}$ J·K^{-1}), T is the temperature (298 K for DOSY experiment), η is the solvent viscosity (0.334 cP for acetonitrile at 298 K), and r is the radius of the molecule (assuming the molecule is a sphere).

Supplementary Figures for Single-Metal ESI-TOF-MS Experiments
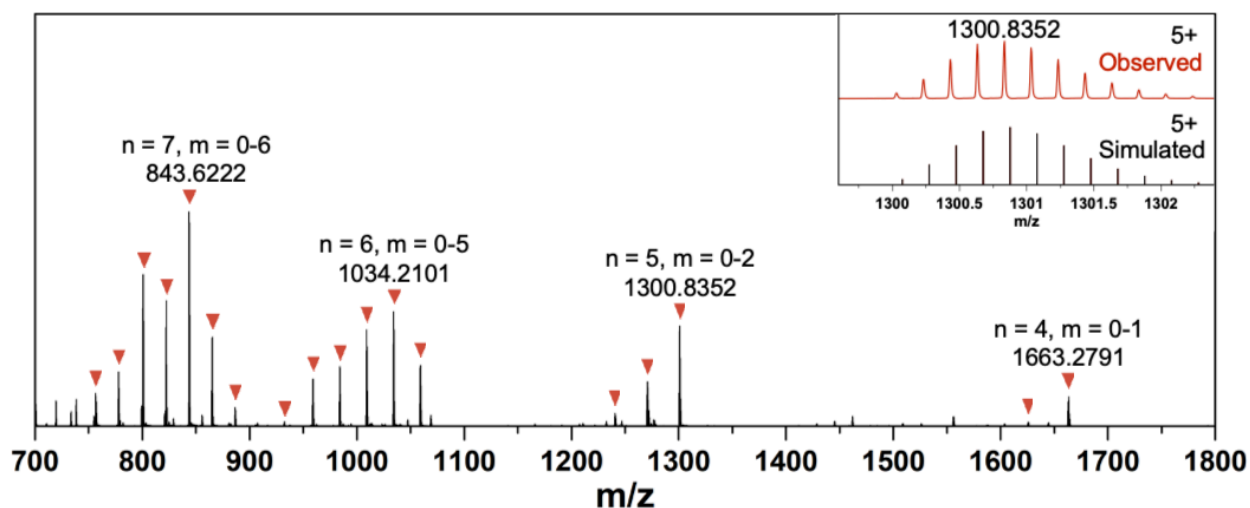
Fig. S23. ESI-TOF-MS spectrum of the Y_4L_4 cage with insets showing the observed and simulated isotopic patterns corresponding to $[Y_4L_4(OTf)_7]^{5+}$. The MS spectrum was analyzed based on the equation $[Y_4L_4(OTf)_{12-n-m}-mH]^{n+}$. For example, peaks with m/z equal to 1663.2791, 1300.8352, 1034.2101, and 843.6222 could be assigned to the charged molecular formulas $[Y_4L_4(OTf)_8]^{4+}$, $[Y_4L_4(OTf)_7]^{5+}$, $[Y_4L_4(OTf)_5-1H]^{6+}$, and $[Y_4L_4(OTf)_3-2H]^{7+}$.
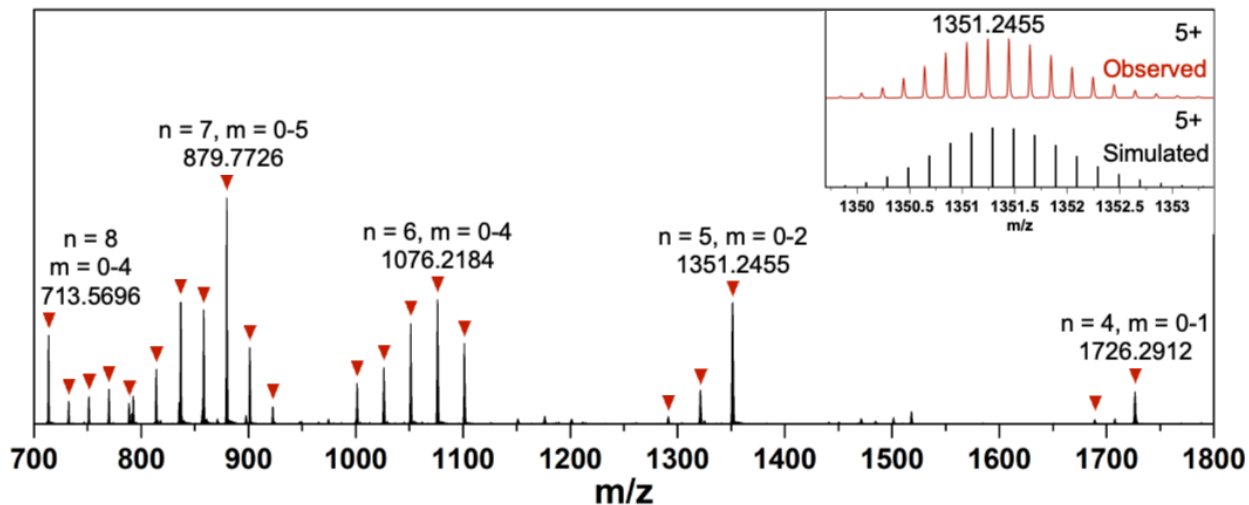
Fig. S24. ESI-TOF-MS spectrum of the Eu_4L_4 cage with insets showing the observed and simulated isotopic patterns corresponding to $[Eu_4L_4(OTf)_7]^{5+}$. The MS spectrum was analyzed based on the equation $[Eu_4L_4(OTf)_{12-n-m}-mH]^{n+}$. For example, peaks with m/z equal to 1726.2912, 1351.2455, 1076.2184, 879.7726, and 713.5696 could be assigned to the charged molecular formulas $[Eu_4L_4(OTf)_8]^{4+}$, $[Eu_4L_4(OTf)_7]^{5+}$, $[Eu_4L_4(OTf)_5-1H]^{6+}$, $[Eu_4L_4(OTf)_3-2H]^{7+}$, and $[Eu_4L_4-4H]^{8+}$.
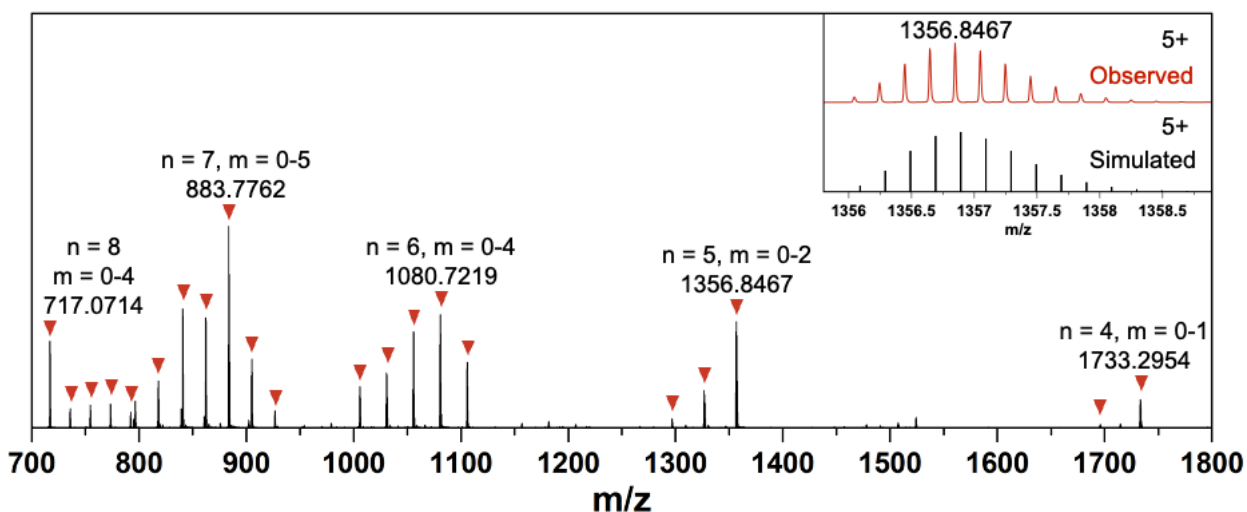
Fig. S25. ESI-TOF-MS spectrum of the Tb_4L_4 cage with insets showing the observed and simulated isotopic patterns corresponding to $[Tb_4L_4(OTf)_7]^{5+}$. The MS spectrum was analyzed based on the

equation $[Tb_4L_4(OTf)_{12-n-m}-mH]^{n+}$. For example, peaks with m/z equal to 1733.2954, 1356.8467, 1080.7219, 883.7762, and 717.0714 could be assigned to the charged molecular formulas $[Tb_4L_4(OTf)_8]^{4+}$, $[Tb_4L_4(OTf)_7]^{5+}$, $[Tb_4L_4(OTf)_5-1H]^{6+}$, $[Tb_4L_4(OTf)_3-2H]^{7+}$, and $[Tb_4L_4-4H]^{8+}$.
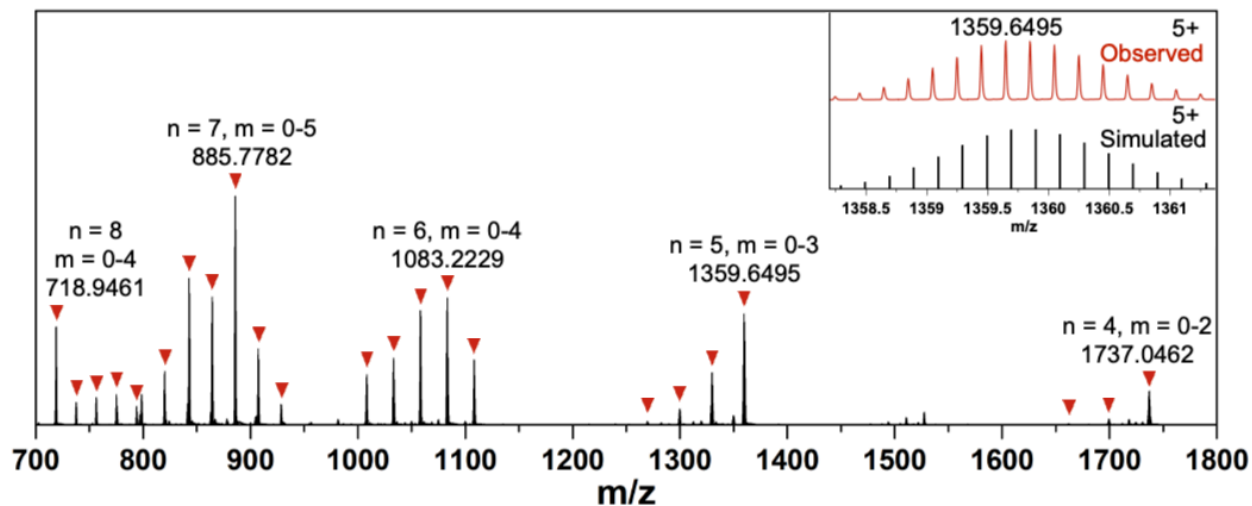
Fig. S26. ESI-TOF-MS spectrum of the Dy_4L_4 cage with insets showing the observed and simulated isotopic patterns corresponding to $[Dy_4L_4(OTf)_7]^{5+}$. The MS spectrum was analyzed based on the equation $[Dy_4L_4(OTf)_{12-n-m}-mH]^{n+}$. For example, peaks with m/z equal to 1737.0462, 1359.6495, 1083.2229, 885.7782, and 718.9461 could be assigned to the charged molecular formulas $[Dy_4L_4(OTf)_8]^{4+}$, $[Dy_4L_4(OTf)_7]^{5+}$, $[Dy_4L_4(OTf)_5-1H]^{6+}$, $[Dy_4L_4(OTf)_3-2H]^{7+}$, and $[Dy_4L_4-4H]^{8+}$.
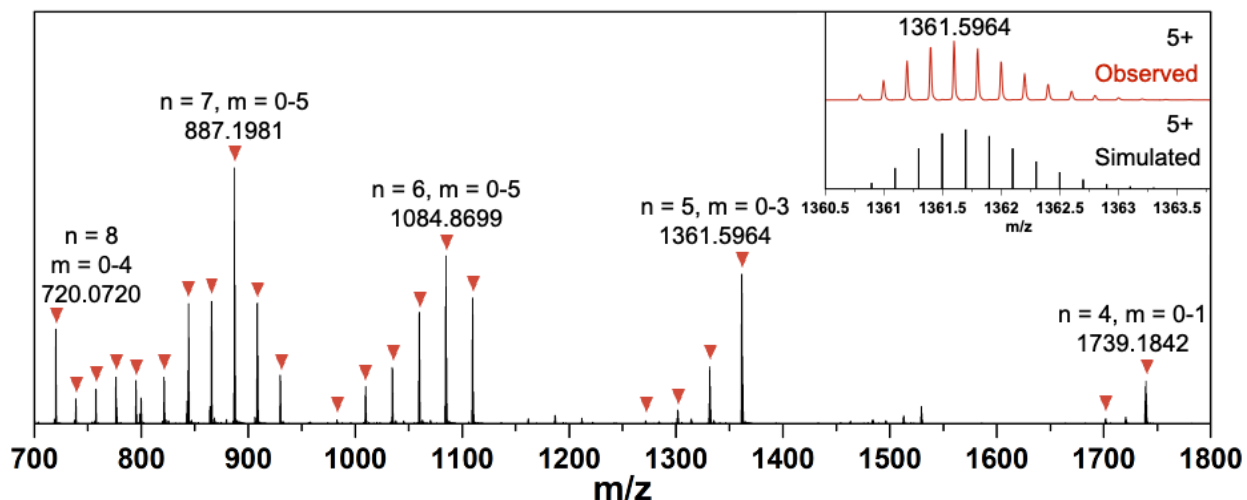
Fig. S27. ESI-TOF-MS spectrum of the Ho_4L_4 cage with insets showing the observed and simulated isotopic patterns corresponding to $[Ho_4L_4(OTf)_7]^{5+}$. The MS spectrum was analyzed based on the equation $[Ho_4L_4(OTf)_{12-n-m}-mH]^{n+}$. For example, peaks with m/z equal to 1739.1842, 1361.5964, 1084.8699, 887.1981, and 720.0720 could be assigned to the charged molecular formulas $[Ho_4L_4(OTf)_8]^{4+}$, $[Ho_4L_4(OTf)_7]^{5+}$, $[Ho_4L_4(OTf)_5-1H]^{6+}$, $[Ho_4L_4(OTf)_3-2H]^{7+}$, and $[Ho_4L_4-4H]^{8+}$.
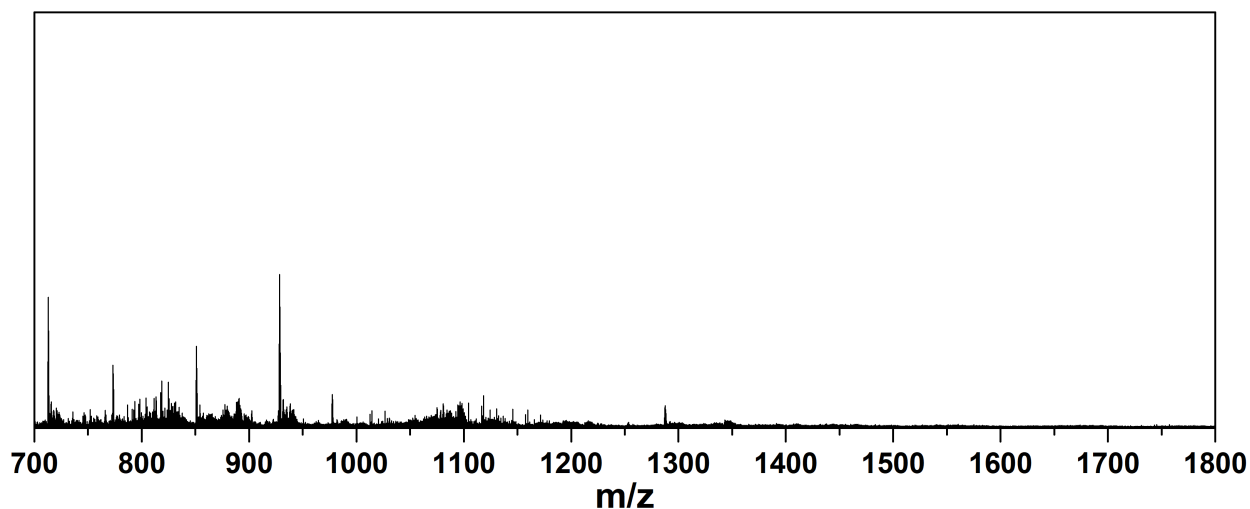
Fig. S28. ESI-TOF-MS spectrum of attempted synthesis of La_4L_4 with the mixture of $La(OTf)_3$ and **L**.

Supplementary Figures for Solid-State NMR Experiments
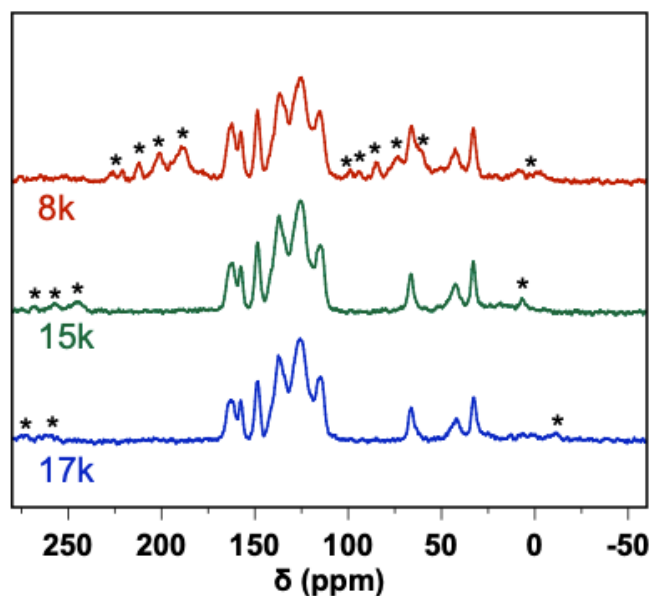
Fig. S29. Solid-state ^{13}C NMR spectra of **L** with 8k (red), 15k (green), and 17k (blue) spin rates. Side bands have been labelled with asterisks (*).
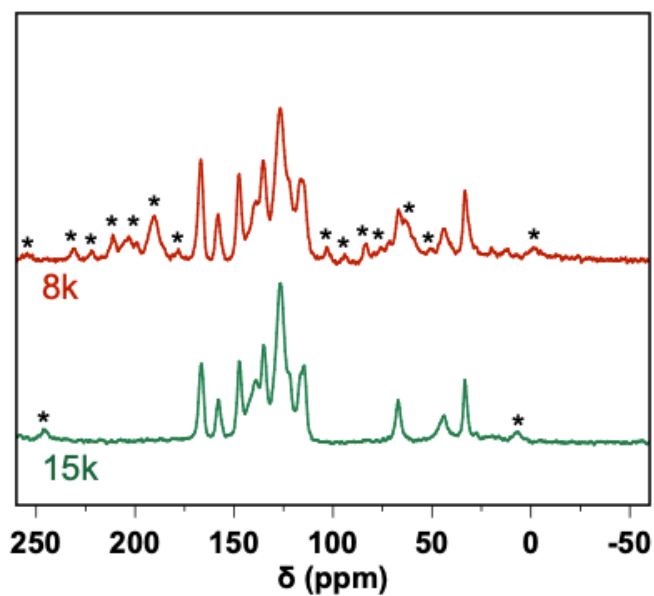
Fig. S30. Solid-state ^{13}C NMR spectra of Y_4L_4 with 8k (red) and 15k (green) spin rates. Side bands have been labelled with asterisks (*).
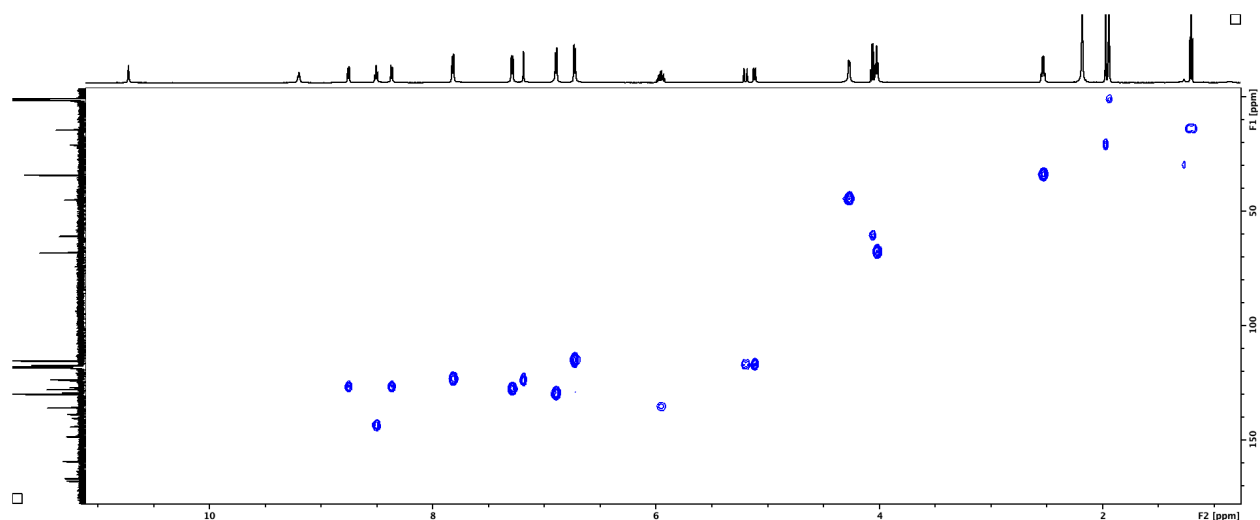
Fig. S31. HSQC NMR spectrum of Y_4L_4 cage (600 MHz, CD_3CN, 298 K).
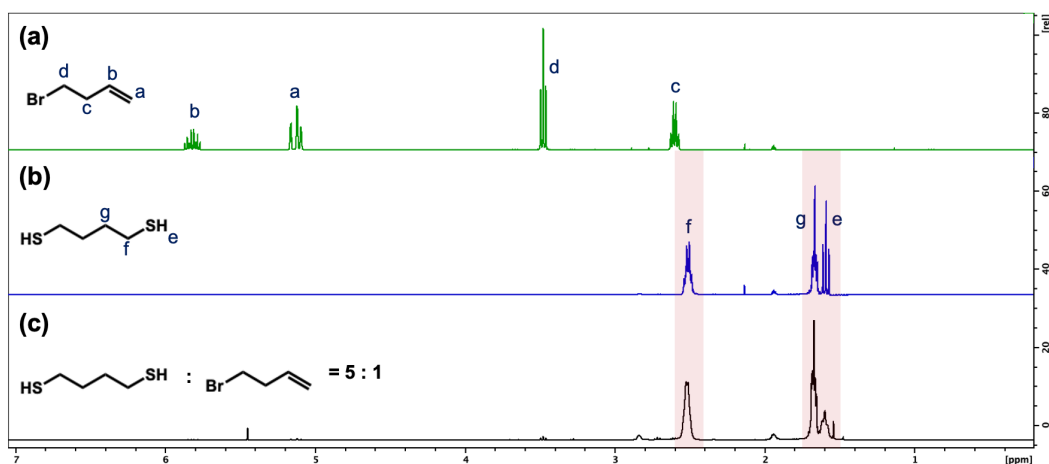
Fig. S32. ^{1}H NMR spectra of (a) 4-bromobut-1-ene, (b) 1,4-butanedithiol, and (c) crude reaction mixtures. (400 MHz, acetonitrile-d_3, 298 K). The procedure for the control experiment was as follows. We reacted 1 equivalent of this small-molecule alkene with 5 equivalents of 1,4-butanedithiol to examine whether disulfide bonds would form in a system with a 10-fold excess of thiol, and the results were examined by NMR (Fig. S32). The reaction conditions were as follows: 4-bromobut-1-ene (24.3 mg, 0.18 mmol, 1.0 equiv), 1,4-butanedithiol (110 mg, 0.9 mmol, 5.0 equiv), and azobisisobutyronitrile (AIBN; 1.2 mg, 5% weight percent per vinyl group), and deuterated acetonitrile (2.0 mL) were combined in a single-neck round-bottom flask. The flask was equipped with a condenser, and the mixture was stirred at 70 °C

overnight. The reaction mixture was then cooled to room temperature, and a crude NMR spectrum was collected as shown in Fig. S32(c). The NMR peaks labelled as **e,f**, and **g** in 1,4-butanedithiol are aligned with the peaks in the crude reaction mixture, suggesting the excess of dithiol did not convert into disulfide bond, instead, remaining as 1,4-butanedithiol. Thus, this control experiment supports our conclusion that in the cage network formation (1:10 alkene:thiol system), the cages were functionalized with terminal thiol as well as partially cross-linked, instead of forming disulfide bonds.

Supplementary Table for Effective Ionic Radii and Calculations of Radius Ratios

Table S1. The effective metal ionic radius of each M^{3+} ion, with coordination number of nine.[7]

Metal ions	La^{3+}	Eu^{3+}	Tb^{3+}	Dy^{3+}	Y^{3+}	Ho^{3+}
Effective ionic radii (Å)	1.216	1.120	1.095	1.083	1.075	1.072

Calculations of Radius Ratios: The information on effective ionic radius of each M^{3+} ion, with coordination number of nine, is based on previous literature;[7] the values are summarized in Table S1. The calculation of the ratio between two M^{3+} ions is based on the equation $(M_a-M_b)/(M_b) * 100 \%$, where M_a is the effective ionic radius of the larger rare-earth metal ion and M_b is the effective ionic radius of the smaller rare-earth metal ion.

Supplementary Figures for Mixed-Metal ESI-TOF-MS Experiments
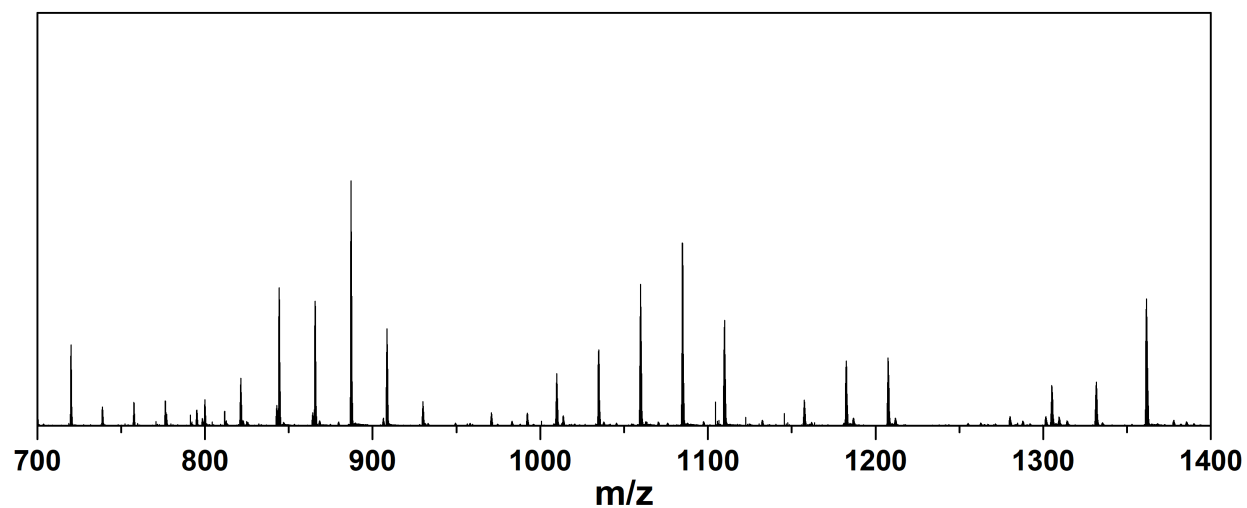
Fig. S33. ESI-TOF-MS spectrum for self-assembly of **L** with La^{3+}/Ho^{3+}.
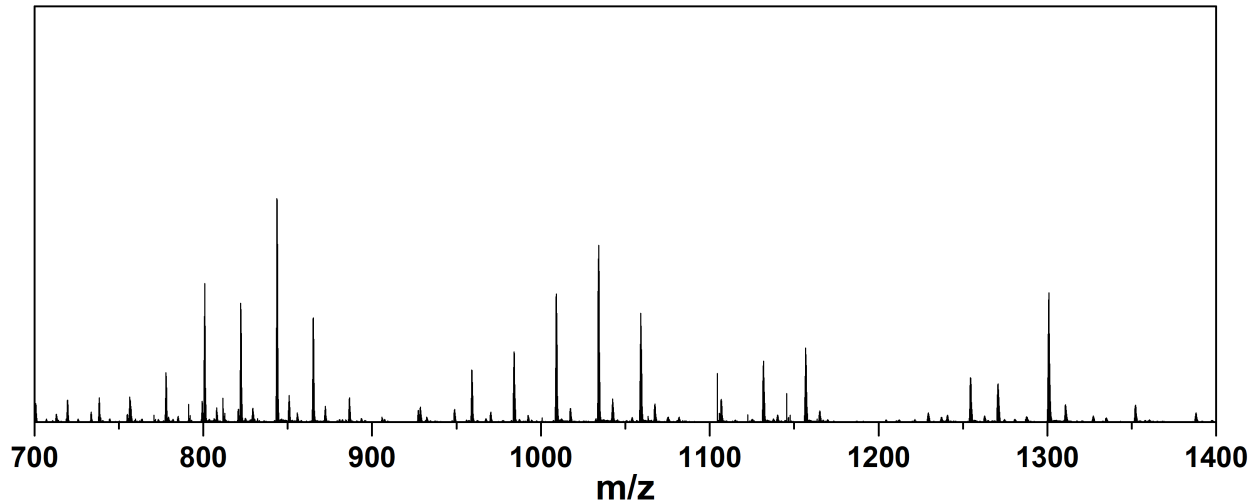
Fig. S34. ESI-TOF-MS spectrum for self-assembly of **L** with La^{3+}/Y^{3+}.
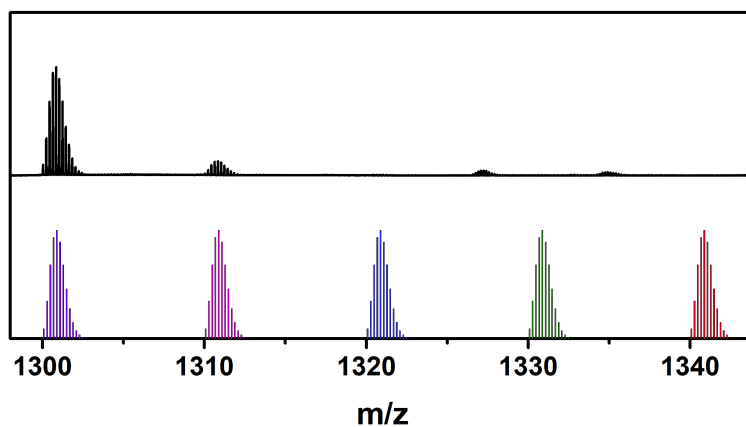
Fig. S35. Top: Partial ESI-TOF-MS spectrum for self-assembly of **L** with La^{3+}/Y^{3+}. Bottom: Simulated isotopic patterns corresponding to $[La_4L_4(OTf)_7]^{5+}$ (red), $[La_3YL_4(OTf)_7]^{5+}$ (green), $[La_2Y_2L_4(OTf)_7]^{5+}$ (blue), $[LaY_3L_4(OTf)_7]^{5+}$ (pink), and $[Y_4L_4(OTf)_7]^{5+}$ (purple).
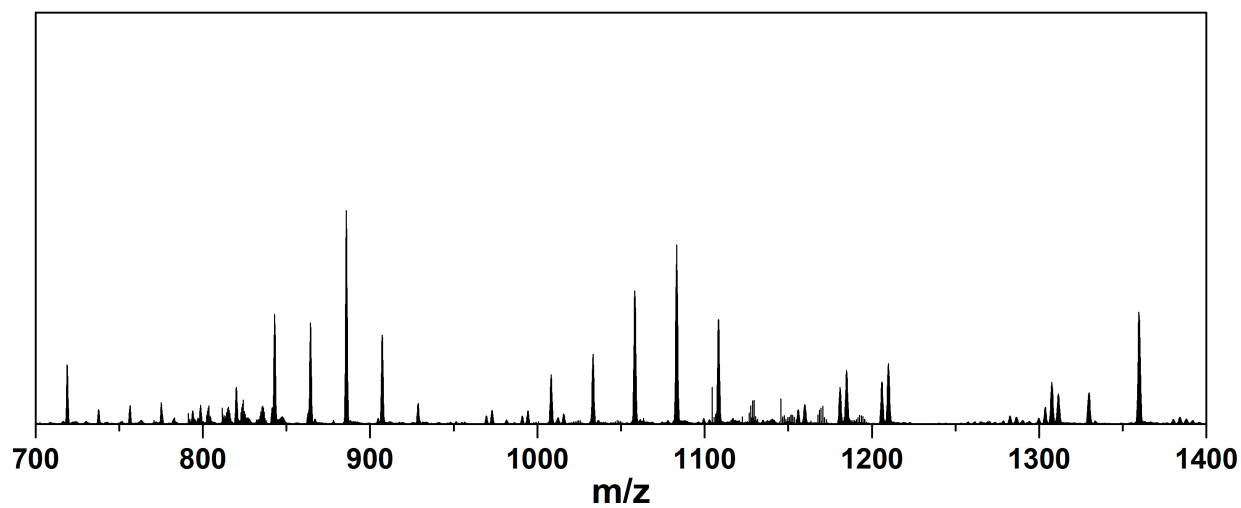
Fig. S36. ESI-TOF-MS spectrum for self-assembly of **L** with La^{3+}/Dy^{3+}.
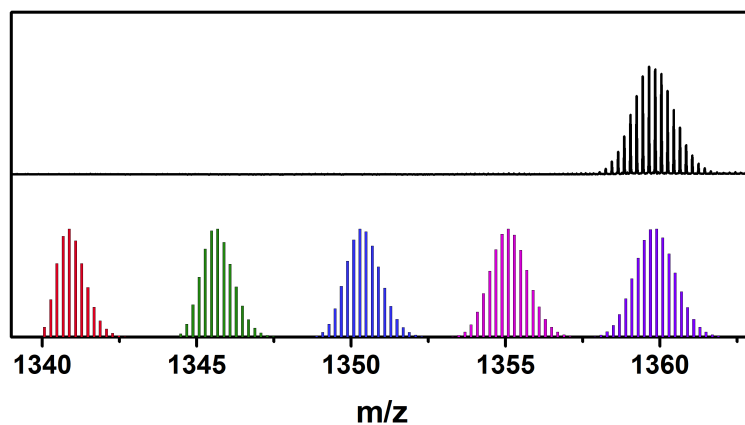
Fig. S37. Top: Partial ESI-TOF-MS spectrum for self-assembly of **L** with La^{3+}/Dy^{3+}. Bottom: Simulated isotopic patterns corresponding to $[La_4L_4(OTf)_7]^{5+}$ (red), $[La_3DyL_4(OTf)_7]^{5+}$ (green), $[La_2Dy_2L_4(OTf)_7]^{5+}$ (blue), $[LaDy_3L_4(OTf)_7]^{5+}$ (pink), and $[Dy_4L_4(OTf)_7]^{5+}$ (purple).
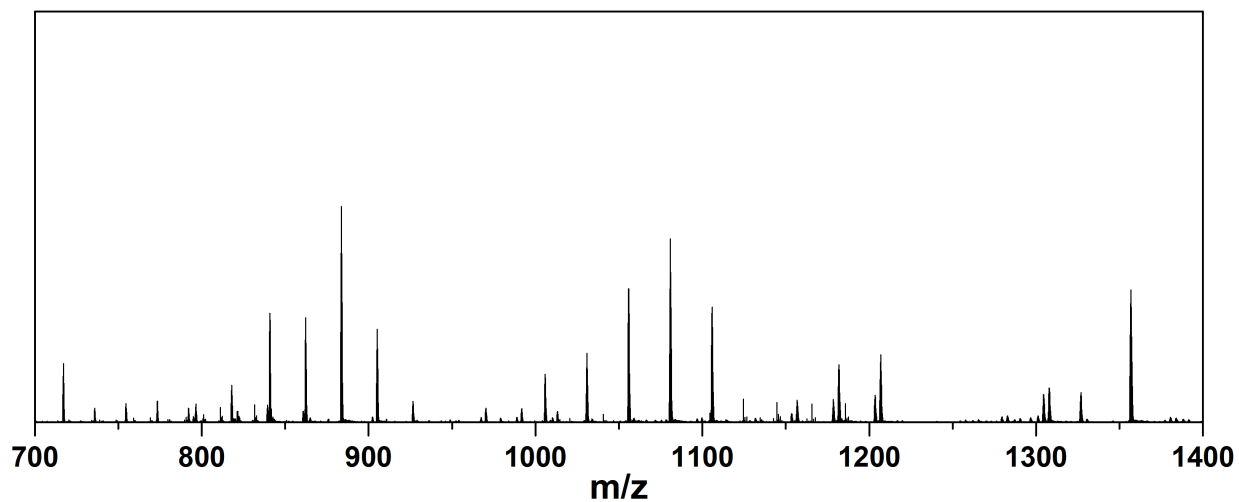
Fig. S38. ESI-TOF-MS spectrum for self-assembly of **L** with La^{3+}/Tb^{3+}.
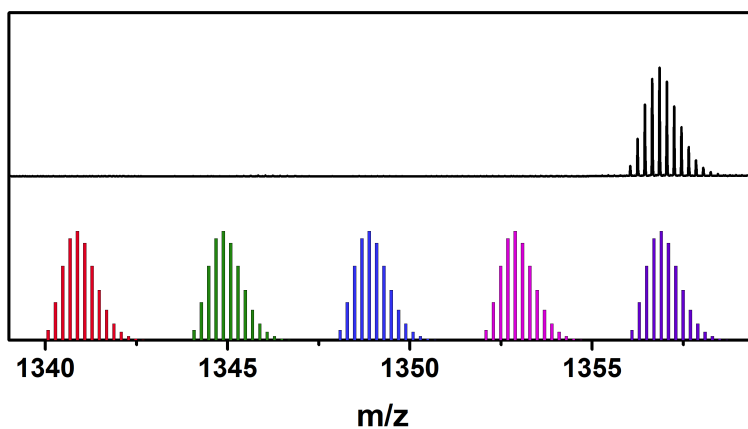
Fig. S39. Top: Partial ESI-TOF-MS spectrum for self-assembly of **L** with La^{3+}/Tb^{3+}. Bottom: Simulated isotopic patterns corresponding to $[La_4L_4(OTf)_7]^{5+}$ (red), $[La_3TbL_4(OTf)_7]^{5+}$ (green), $[La_2Tb_2L_4(OTf)_7]^{5+}$ (blue), $[LaTb_3L_4(OTf)_7]^{5+}$ (pink), and $[Tb_4L_4(OTf)_7]^{5+}$ (purple).
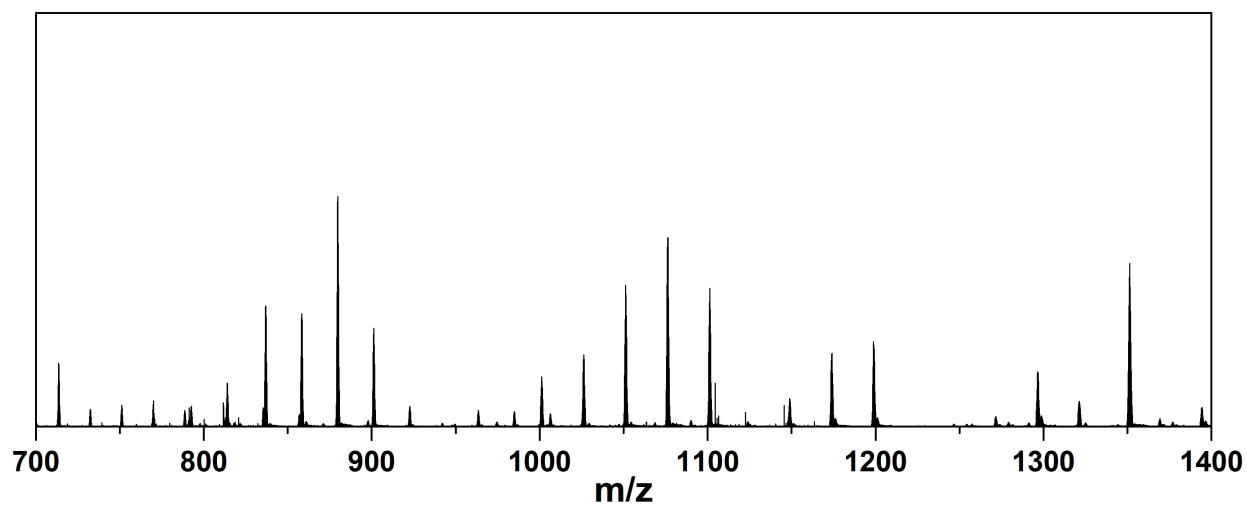
Fig. S40. ESI-TOF-MS spectrum for self-assembly of **L** with La^{3+}/Eu^{3+}.
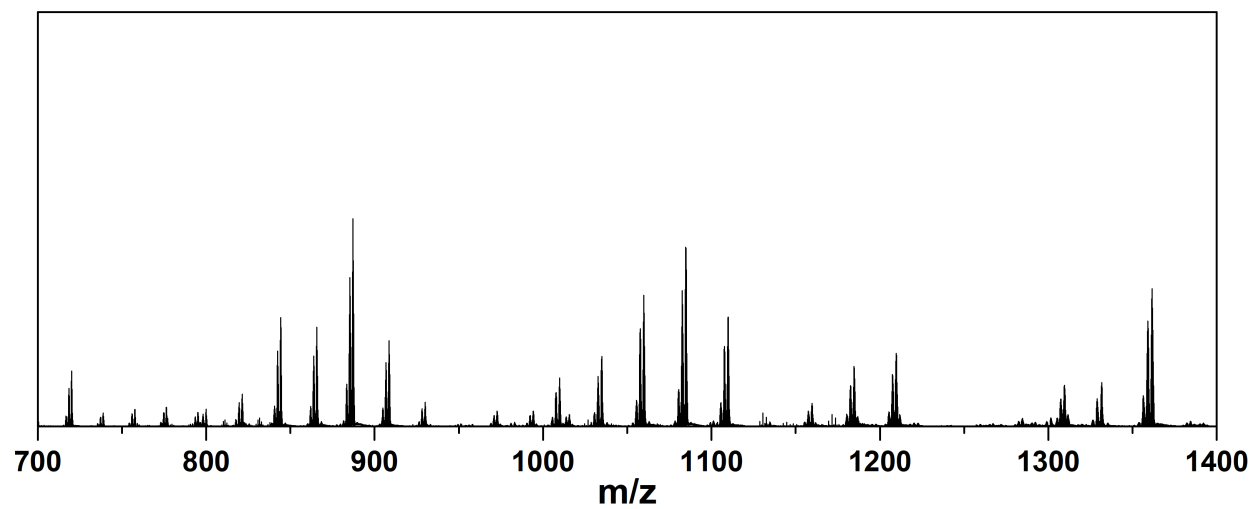
Fig. S41. ESI-TOF-MS spectrum for self-assembly of **L** with Eu^{3+}/Ho^{3+}.
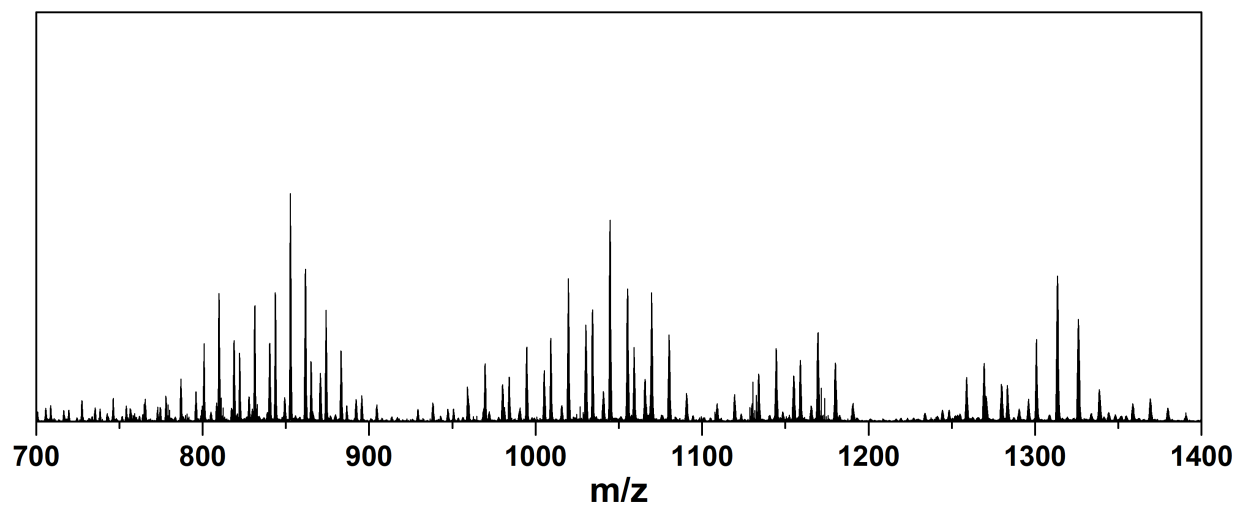
Fig. S42. ESI-TOF-MS spectrum for self-assembly of **L** with Eu^{3+}/Y^{3+}.
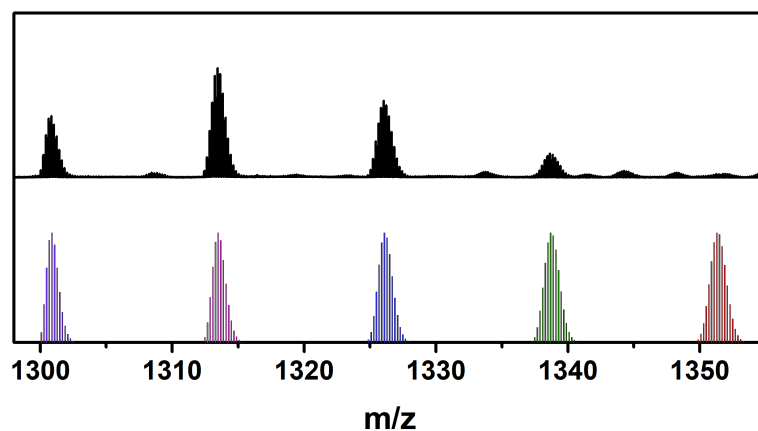
Fig. S43. Top: Partial ESI-TOF-MS spectrum for self-assembly of **L** with Eu^{3+}/Y^{3+}. Bottom: Simulated isotopic patterns corresponding to $[Eu_4L_4(OTf)_7]^{5+}$ (red), $[Eu_3YL_4(OTf)_7]^{5+}$ (green), $[Eu_2Y_2L_4(OTf)_7]^{5+}$ (blue), $[EuY_3L_4(OTf)_7]^{5+}$ (pink), and $[Y_4L_4(OTf)_7]^{5+}$ (purple).
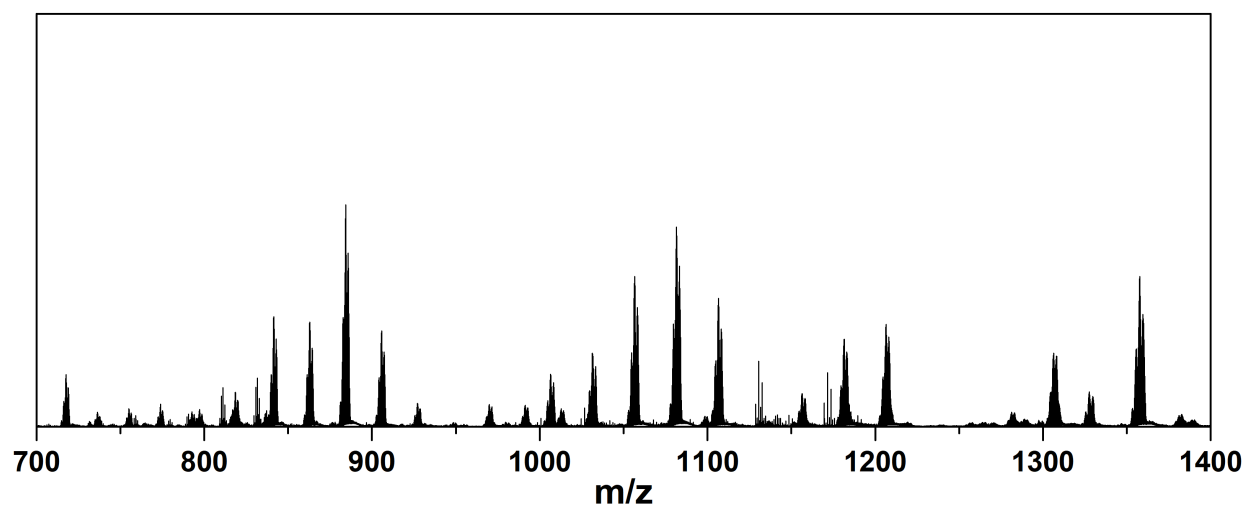
Fig. S44. ESI-TOF-MS spectrum for self-assembly of **L** with Eu^{3+}/Dy^{3+}.
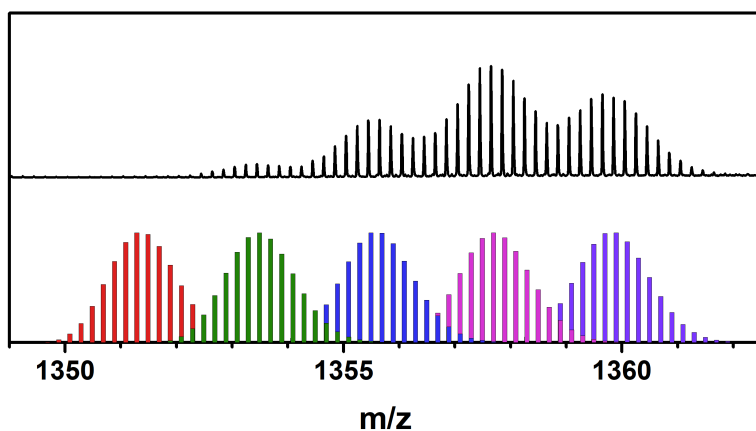
Fig. S45. Top: Partial ESI-TOF-MS spectrum for self-assembly of **L** with Eu^{3+}/Dy^{3+}. Bottom: Simulated isotopic patterns corresponding to $[Eu_4L_4(OTf)_7]^{5+}$ (red), $[Eu_3DyL_4(OTf)_7]^{5+}$ (green), $[Eu_2Dy_2L_4(OTf)_7]^{5+}$ (blue), $[EuDy_3L_4(OTf)_7]^{5+}$ (pink), and $[Dy_4L_4(OTf)_7]^{5+}$ (purple).
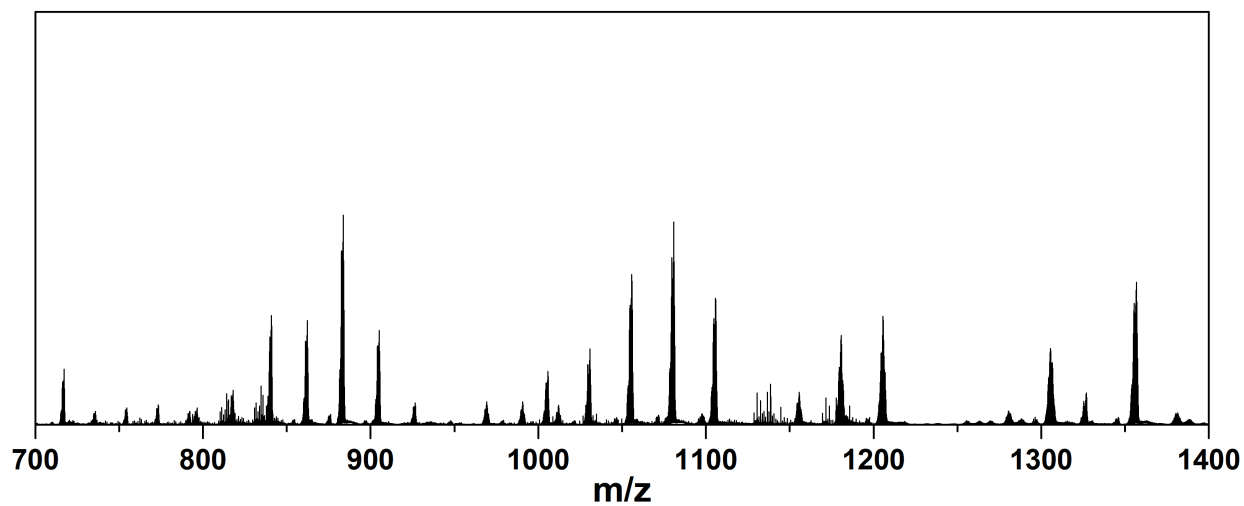
Fig. S46. ESI-TOF-MS spectrum for self-assembly of **L** with Eu^{3+}/Tb^{3+}.
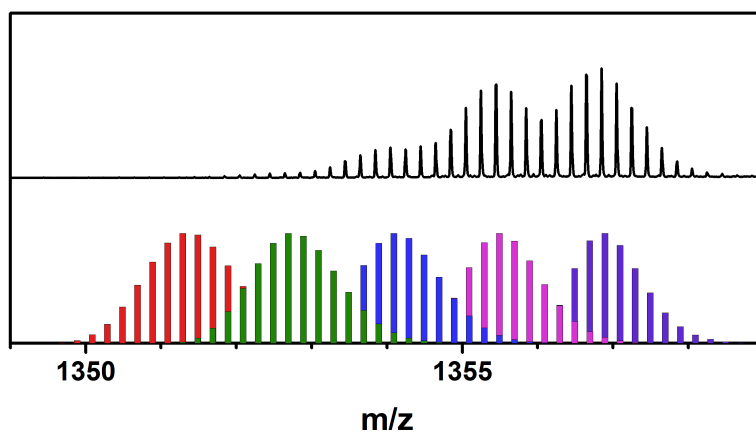
Fig. S47. Top: Partial ESI-TOF-MS spectrum for self-assembly of **L** with Eu^{3+}/Tb^{3+}. Bottom: Simulated isotopic patterns corresponding to $[Eu_4L_4(OTf)_7]^{5+}$ (red), $[Eu_3TbL_4(OTf)_7]^{5+}$ (green), $[Eu_2Tb_2L_4(OTf)_7]^{5+}$ (blue), $[EuTb_3L_4(OTf)_7]^{5+}$ (pink), and $[Tb_4L_4(OTf)_7]^{5+}$ (purple).
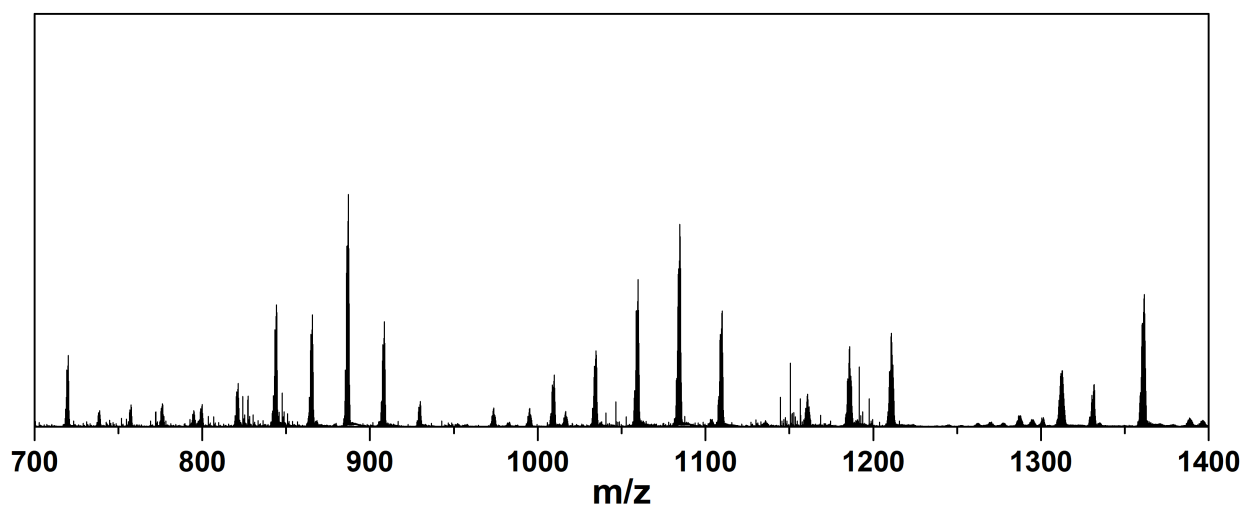
Fig. S48. ESI-TOF-MS spectrum for self-assembly of **L** with Tb^{3+}/Ho^{3+}.
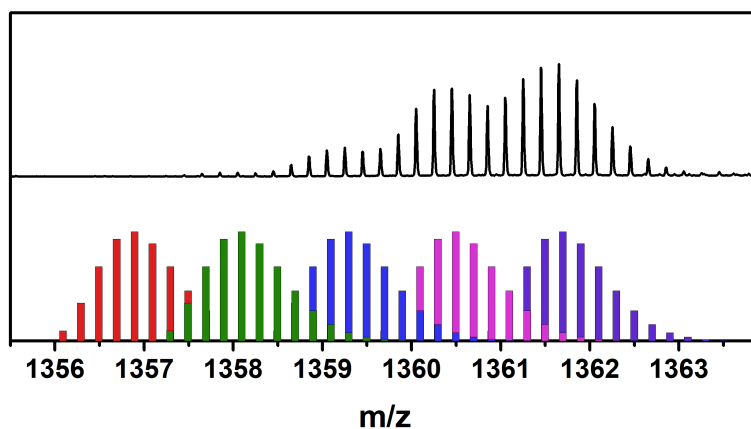
Fig. S49. Top: Partial ESI-TOF-MS spectrum for self-assembly of **L** with Tb^{3+}/Ho^{3+}. Bottom: Simulated isotopic patterns corresponding to [Tb$_4$**L**$_4$(OTf)$_7$]$^{5+}$ (red), [Tb$_3$Ho**L**$_4$(OTf)$_7$]$^{5+}$ (green), [Tb$_2$Ho$_2$**L**$_4$(OTf)$_7$]$^{5+}$ (blue), [TbHo$_3$**L**$_4$(OTf)$_7$]$^{5+}$ (pink), and [Ho$_4$**L**$_4$(OTf)$_7$]$^{5+}$ (purple).
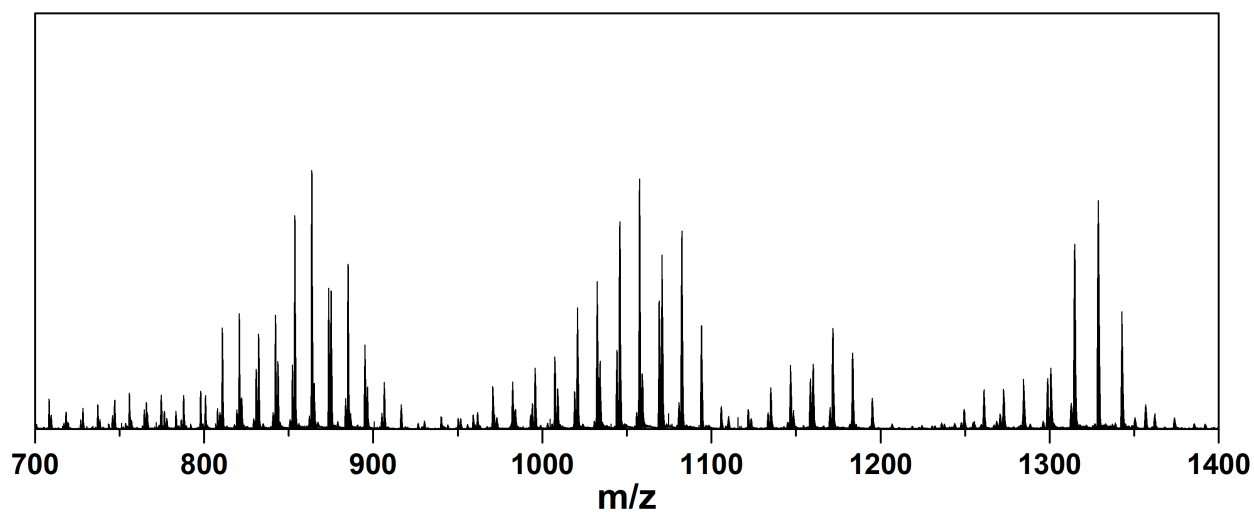
Fig. S50. ESI-TOF-MS spectrum for self-assembly of **L** with Tb^{3+}/Y^{3+}.
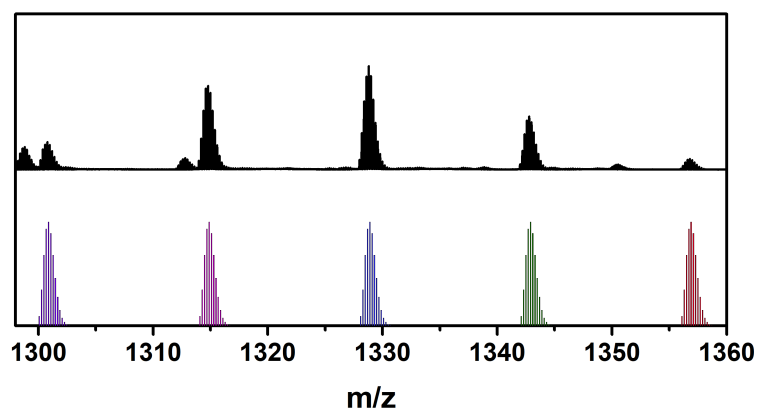
Fig. S51. Top: Partial ESI-TOF-MS spectrum for self-assembly of **L** with Tb^{3+}/Y^{3+}. Bottom: Simulated isotopic patterns corresponding to $[Tb_4L_4(OTf)_7]^{5+}$ (red), $[Tb_3YL_4(OTf)_7]^{5+}$ (green), $[Tb_2Y_2L_4(OTf)_7]^{5+}$ (blue), $[TbY_3L_4(OTf)_7]^{5+}$ (pink), and $[Y_4L_4(OTf)_7]^{5+}$ (purple).
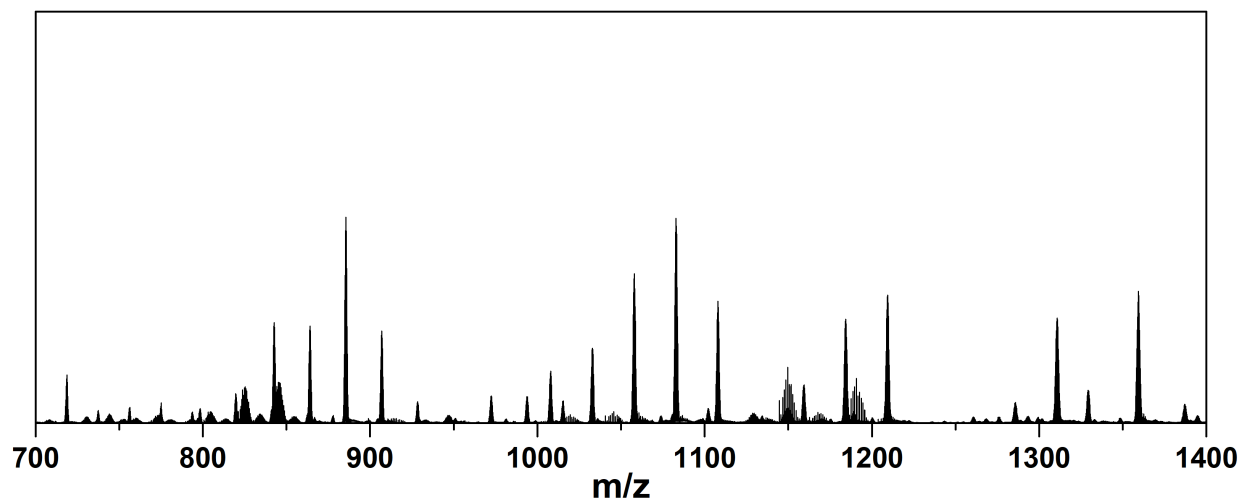
Fig. S52. ESI-TOF-MS spectrum for self-assembly of **L** with Tb^{3+}/Dy^{3+}.
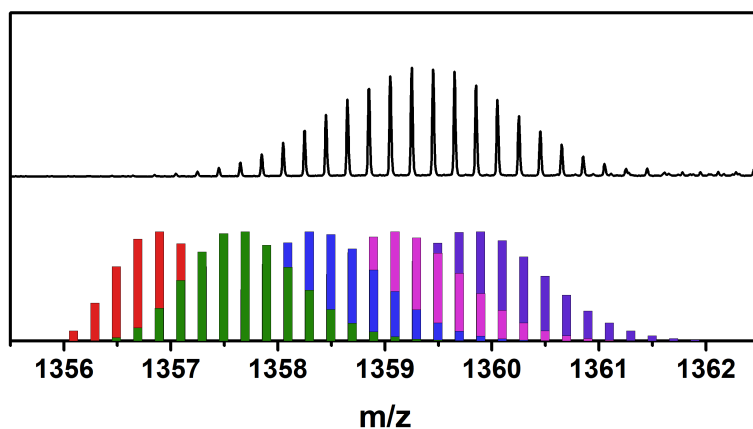
Fig. S53. Top: Partial ESI-TOF-MS spectrum for self-assembly of **L** with Tb^{3+}/Dy^{3+}. Bottom: Simulated isotopic patterns corresponding to $[Tb_4L_4(OTf)_7]^{5+}$ (red), $[Tb_3DyL_4(OTf)_7]^{5+}$ (green), $[Tb_2Dy_2L_4(OTf)_7]^{5+}$ (blue), $[TbDy_3L_4(OTf)_7]^{5+}$ (pink), and $[Dy_4L_4(OTf)_7]^{5+}$ (purple).
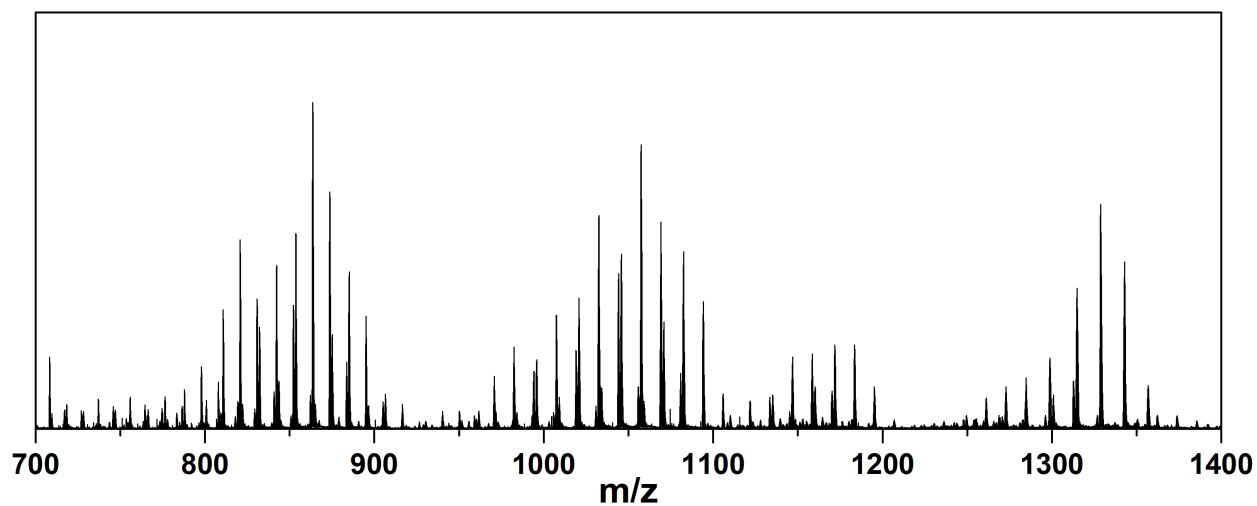
Fig. S54. ESI-TOF-MS spectrum for self-assembly of **L** with Dy^{3+}/Y^{3+}.
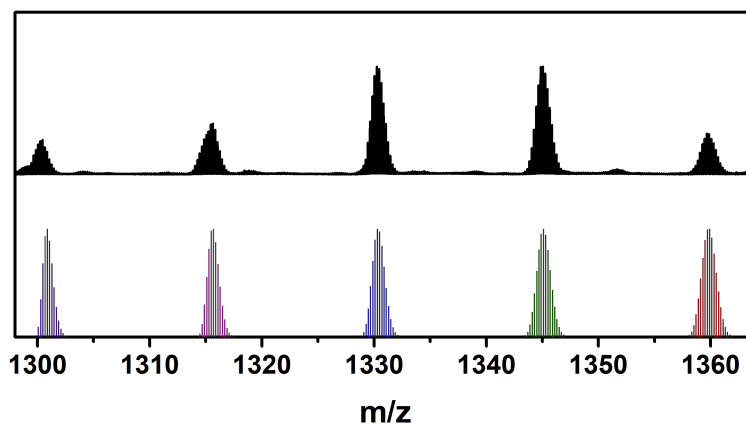
Fig. S55. Top: Partial ESI-TOF-MS spectrum for self-assembly of **L** with Dy^{3+}/Y^{3+}. Bottom: Simulated isotopic patterns corresponding to $[Dy_4L_4(OTf)_7]^{5+}$ (red), $[Dy_3YL_4(OTf)_7]^{5+}$ (green), $[Dy_2Y_2L_4(OTf)_7]^{5+}$ (blue), $[DyY_3L_4(OTf)_7]^{5+}$ (pink), and $[Y_4L_4(OTf)_7]^{5+}$ (purple).
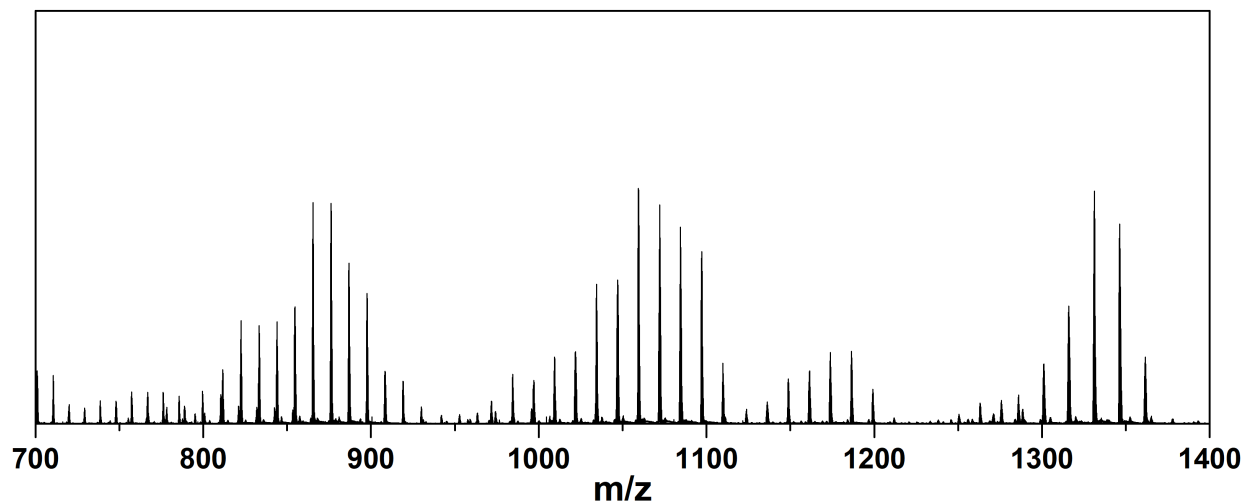
Fig. S56. ESI-TOF-MS spectrum for self-assembly of **L** with Y^{3+}/Ho^{3+}.

Supplementary Table and Figures for Rare-Earth Batch Experiments

Table S2. Summary of the conditions and results of the adsorption experiments.

	Scaffold (1:1) Y^{3+} only	Scaffold (1:1) La^{3+} only	Scaffold (1:1) Y^{3+} /La^{3+}	Scaffold (1:10) Y^{3+} only	Scaffold (1:10) La^{3+} only	Scaffold (1:10) Y^{3+} /La^{3+}
Weights of scaffolds (mg)	14.1	14.4	15.9	14.3	14.1	14.7
Weights of stock solutions (mg)	479	489.5	485.7	484.1	483	483.9
Y^{3+} removal (%)	46.7	N/A	73.5	29.6	N/A	52.8
La^{3+} removal (%)	N/A	88.6	37.4	N/A	87.9	47.4

Concentrations of Rare-Earth Stock Solutions: The concentration of rare-earth ions from the supernatants of the batch experiments and the stock solutions were determined by MP-AES. The concentration of Y^{3+} was 2126 µg/g in the pure Y^{3+} stock solution. The concentration of La^{3+} was 4174 µg/g in the pure La^{3+} stock solution. The concentration of Y^{3+} was 2237 µg/g and the concentration of La^{3+} was 3736 µg/ g in the Y^{3+}/La^{3+} stock solution.
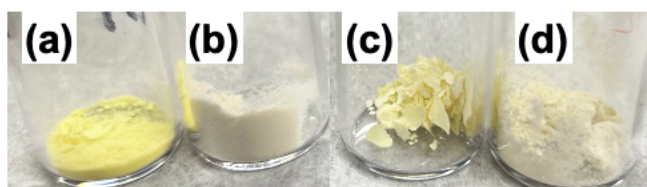
Fig. S57. Photos of **(a)** network of Y_4L_4 cages (1:1 alkene:thiol), **(b)** network of Y_4L_4 cages (1:10 alkene:thiol), **(c)** the demetallated network scaffold from the network of Y_4L_4 cages (1:1 alkene:thiol), denoted as scaffold (1:1), and **(d)** the demetallated network scaffold from the network of Y_4L_4 cages (1:10 alkene:thiol), denoted as scaffold (1:10).
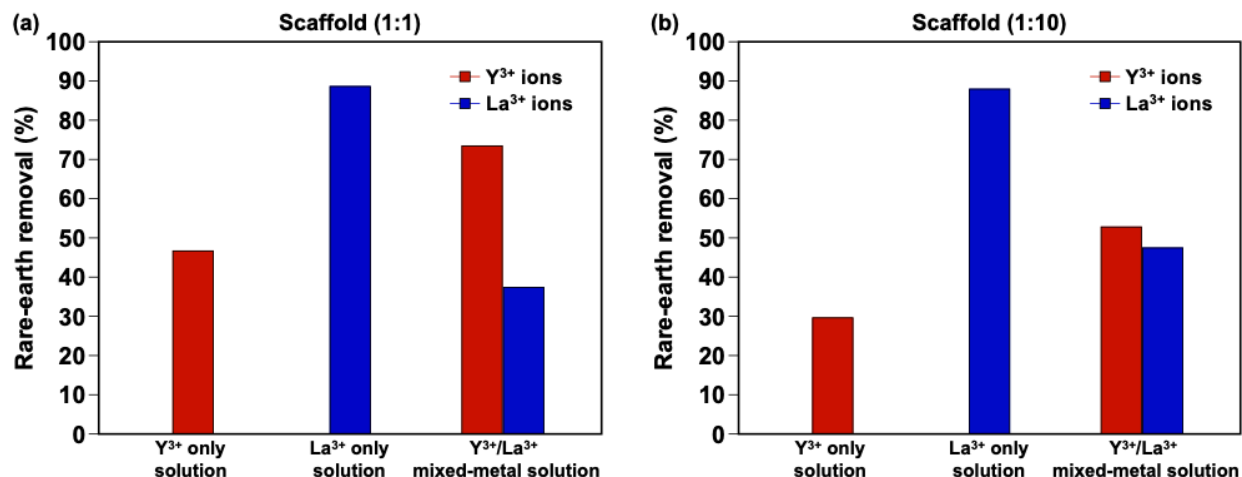
Fig. S58. The rare-earth removal (%) of pure Y^{3+} solution, pure La^{3+} solution, and Y^{3+}/La^{3+} mixed-ion solution adsorbed by **(a)** scaffold (1:1) and **(b)** scaffold (1:10).

References

1. M. Sanguinetti, S. Sanfilippo, D. Castagnolo, D. Sanglard, B. Posteraro, G. Donzellini and M. Botta, *ACS Med. Chem. Lett.*, 2013, **4**, 852–857.

2. J.-T. Ou, M. K. Brown, J. D. Kaff, R. W. Hughes, D. L. Huber, B. S. Sumerlin, K. I. Winey and M. K. Taylor, *ACS Appl. Polym. Mater.*, 2024, **6**, 11420–11426.

3. Q.-Q. Yan, L.-P. Zhou, H.-Y. Zhou, Z. Wang, L.-X. Cai, X.-Q. Guo, X.-Q. Sun and Q.-F. Sun, *Dalton Trans.*, 2019, **48**, 7080–7084.

4. Y. Zhang, Y. Zhao, C. Zhang, X. Luo and X. Liu, *CrystEngComm*, 2022, **24**, 4496–4499.

5. A. de la P. Ruigómez, D. Rodríguez-San-Miguel, K. C. Stylianou, M. Cavallini, D. Gentili, F. Liscio, S. Milita, O. M. Roscioni, M. L. Ruiz-González, C. Carbonell, D. Maspoch, R. Mas-Ballesté, J. L. Segura and F. Zamora, *Chem. Eur. J.*, 2015, **21**, 10666–10670.

6. X.-Z. Li, L.-P. Zhou, L.-L. Yan, Y.-M. Dong, Z.-L. Bai, X.-Q. Sun, J. Diwu, S. Wang, J.-C. Bünzli and Q.-F. Sun, *Nat. Commun.*, 2018, **9**, 547.

7. R. D. Shannon, *Acta Cryst.*, 1976, **32**, 751–767.